Quaternary Research

doi:10.1017/qua.2019.76

The "missing glaciations" of the Middle Pleistocene

Philip D. Hughes[a]*, Philip L. Gibbard[b], Jürgen Ehlers[c]

[a]Department of Geography, School of Environment, Education and Development, University of Manchester, Oxford Road, Manchester M13 9PL, United Kingdom
[b]Scott Polar Research Institute, University of Cambridge, Cambridge CB2 1ER, United Kingdom
[c]Hellberg 2a, D-21514 Witzeeze, Germany
*Corresponding author e-mail address: philip.hughes@manchester.ac.uk (P.D. Hughes).

(Received January 16, 2019; Accepted October 30, 2019)

Abstract

Global glaciations have varied in size and magnitude since the Early–Middle Pleistocene transition (~773 ka), despite the apparent regular and high-amplitude 100 ka pacing of glacial–interglacial cycles recorded in marine isotope records. The evidence on land indicates that patterns of glaciation varied dramatically between different glacial–interglacial cycles. For example, Marine Isotope Stages (MIS) 8, 10, and 14 are all noticeably absent from many terrestrial glacial records in North America and Europe. However, globally, the patterns are more complicated, with major glaciations recorded in MIS 8 in Asia and in parts of the Southern Hemisphere, such as Patagonia, for example. This spatial variability in glaciation between glacial–interglacial cycles is likely to be driven by ice volume changes in the West Antarctic Ice Sheet and associated interhemispheric connections through ocean–atmosphere circulatory changes. The weak global glacial imprint in some glacial–interglacial cycles is related to the pattern of global ice buildup. This is caused by feedback mechanisms within glacial systems themselves that partly result from long-term orbital changes driven by eccentricity.

Keywords: ice ages; glacial cycles; orbital forcing; Saalian; Wolstonian; Illinoian; Quaternary stratigraphy

INTRODUCTION

The most extensive and sustained glaciations in the Quaternary began in the last 900 ka (ca. Marine Isotope Stages [MIS] 24–22 to present) in the Northern Hemisphere and are associated with 100 ka eccentricity-driven glacial–interglacial cycles (Head and Gibbard, 2015; Hughes and Gibbard, 2018). Despite the obliquity-driven shorter 41 ka glacial–interglacial cycles of the earlier Pleistocene, there is evidence that high- and mid-latitudinal ice sheets in the North Atlantic region have been present since the beginning of the Pleistocene (Thierens et al., 2012). Southern Hemisphere glaciation is an even longer-established phenomenon, with substantial glaciation already a regular occurrence in the Tertiary (Ehlers et al., 2018).

In the Italian Dolomites, glaciation became established in MIS 22 (Muttoni et al., 2003). Comparable evidence is also found north of the Alps in Switzerland and southern Germany (Fiebig et al., 2011). However, the "Deckenschotter" glaciofluvial deposits in Switzerland may represent earlier glaciation, and the older "Höhere Deckenschotter" include vertebrate remains that suggest an age of 2.6–1.8 Ma (Bolliger et al., 1996). The "Höhere Deckenschotter" are regarded as glaciofluvial deposits. However, no till has been found as yet. In contrast, the "Tiefere Deckenschotter" contain tills. Glaciation during that time might have been more extensive than in the Würmian—see Figure 1 for global chronostratigraphic correlations. The age is uncertain, but the deposits clearly predate the Middle Pleistocene (Preusser et al., 2011), which Schlüchter (1989) identified as a major phase of geomorphological change ("Mittelpleistozäne Wende") in the the Alps. The oldest glaciation identified in the Pyrenees is of late Cromerian age (MIS 16 or 14) (Calvet, 2004). In North America, widespread lowland glaciation (beyond Alaska and the Northern Territories) is first seen during MIS 22 or 20 (Barendregt and Duk-Rodkin, 2011; Duk-Rodkin and Barendregt, 2011). In South America, the extensive Great Patagonian glaciation is dated to 1.1 Ma and correlated with MIS 30–34 (Singer et al., 2004).

Following the Early Pleistocene precursors, glaciers reached lowland northern Europe and Siberia in the early Middle Pleistocene shortly before end of the Brunhes–Matuyama palaeomagnetic reversal (~773 ka; Singer et al. 2019), which represents the boundary between the Early

Cite this article: Hughes, P. D., Gibbard, P. L., Ehlers, J. 2020. The "missing glaciations" of the Middle Pleistocene. *Quaternary Research* 96, 161–183. https://doi.org/10.1017/qua.2019.76

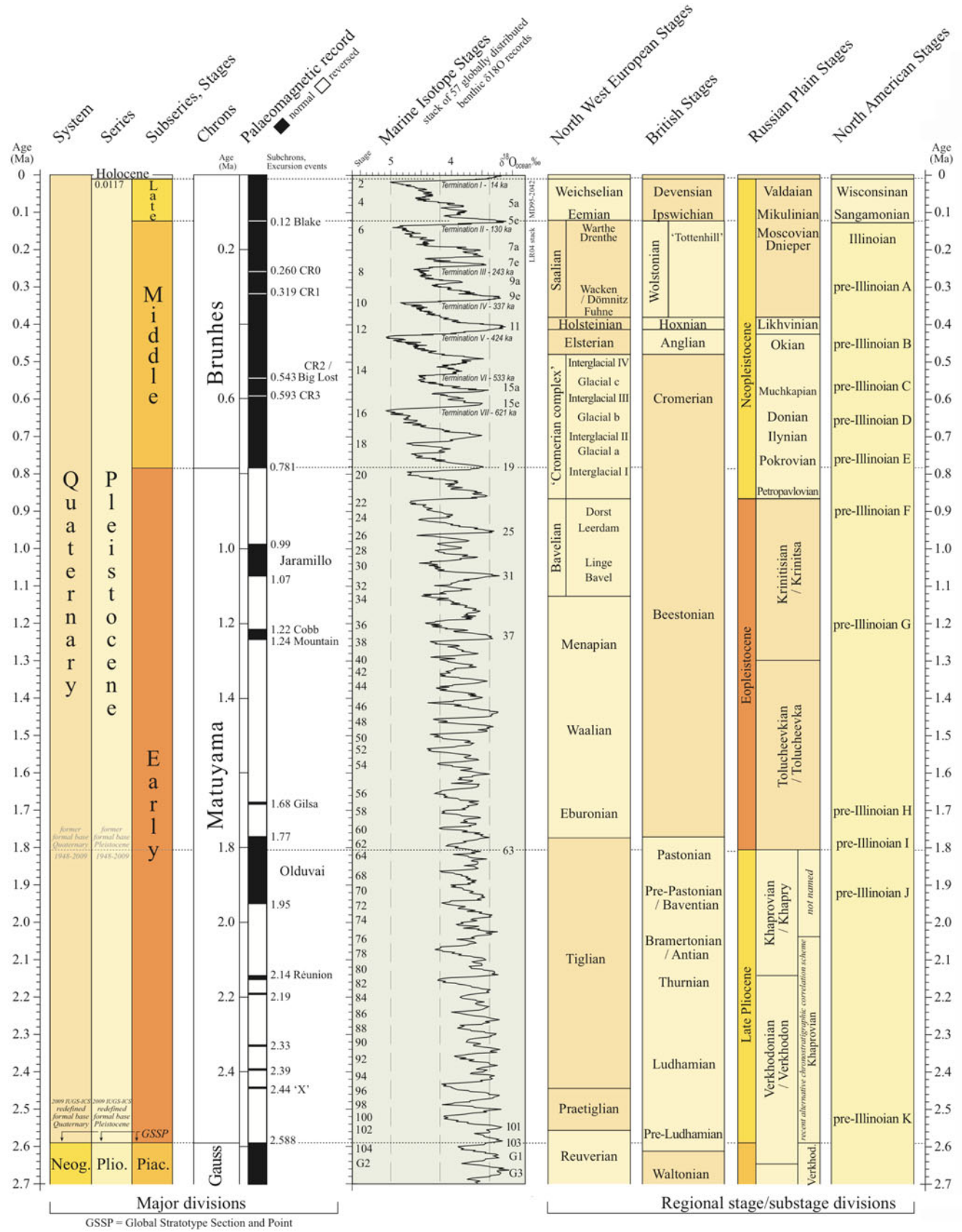

Figure 1. (color online) Global correlations between terrestrial glacial chronostratigraphic terms and the marine oxygen isotope record. Adapted from the global chronostratigraphic correlation table for the past 2.7 million years by Cohen and Gibbard (2011).

https://doi.org/10.1017/qua.2019.76 Published online by Cambridge University Press

and Middle Pleistocene (Head et al., 2008; Head and Gibbard 2015). These events laid down extensive sheets of glaciogenic deposits across wide areas both on land and beneath the sea. In the northern North Sea, the formation of the Norwegian Channel caused an abrupt change of sedimentary conditions at about this time (Ottesen et al., 2014). While 100 ka cycles began ca. MIS 24–22 (Elderfield et al., 2012), the largest-amplitude 100 ka glaciations started with MIS 16, which marked the completion of the Early–Middle Pleistocene transition (Head and Gibbard, 2005; Mudelsee and Schulz, 1997; Hughes and Gibbard, 2018).

Subsequently, major ice sheets repeatedly extended over large regions of North America during the Middle Pleistocene pre-Illinoian events MIS 16, 12, and 6 (Illinoian s.s.) and the Late Pleistocene MIS 5d–2 (Wisconsinan). The Laurentide Ice Sheet formed over large areas of Canada, reaching as far south as 38°N in the United States during the Late Pleistocene (Dyke and Prest, 1987; Fig. 2). More significantly, the change in ice volume between glacial–interglacial cycles was the largest single contribution to the global sea-level changes. This was 70–90 m for the last glacial–interglacial cycle (Stokes et al., 2012), which represents well over half the global ice contribution to glacial–interglacial sea-level change. Today, the largest ice sheet is restricted to Greenland, with much smaller ice caps present in Canada.

The marine oxygen isotope record provides the main basis for defining Quaternary glacial–interglacial cycles (Lisiecki and Raymo, 2005) and has long been considered to represent a record of global ice volume (Shackleton, 1967). The marine isotope record is widely used as the global reference for subdividing the Quaternary, and the scheme of stages and substages in the marine isotope record continues to underpin the Quaternary time scale (Lisiecki and Raymo, 2005; Railsback et al., 2015; Fig. 1). The marine isotope record has the advantage of being derived from quasi-continuous sedimentary sequences on the deep-ocean floors, whereas the glacial records on land are inherently fragmentary. However, the marine isotope record is a composite signal of fluctuations in global ice volume and does not provide information on the spatial pattern of glaciations. Furthermore, because changes in global ice volume are dominated by the Laurentide Ice Sheet (Fig. 2), it is not necessarily representative of the pattern and scale of glaciations in other parts of the world. This poses problems for direct terrestrial–marine correlation (Gibbard and West, 2000), and care must be taken to isolate glacial records using single proxies such as the marine isotope record. This is also true for other indirect proxies for global glaciations, some of which are used here, such as sea-level and ice-core records. Thus, a collective approach is necessary to decipher the patterns of global glaciations, especially where terrestrial glacial records are absent, ambiguous, or poorly dated, which is often the case, especially for the Middle Pleistocene glaciations.

The application of numerical dating of Late Pleistocene glaciations is increasingly demonstrating the asynchronies in the timing of glacial maxima on a global scale (Hughes et al., 2013). While the differing timing of mountain glaciations compared with the continental ice sheets has been known for decades (e.g., Gillespie and Molnar, 1995), there is now also evidence that the timing of maximum extents of major ice sheet margins may have differed by as much as tens of thousands of years. Such differences appear to result from the contrasting regional geographical situations, where differing ocean and atmospheric circulatory patterns influence precipitation and air temperatures (Hughes et al., 2013).

Differences in the pattern and timing of glacial extent are also notable between different glacial–interglacial cycles (cf. Margari et al., 2010, 2014; Hughes and Gibbard, 2018; Batchelor et al., 2019). The largest glaciations of the last 800 ka, such as in MIS 5d-2, were characterized by an early advance of glaciers followed by an interlude, then a second major advance leading to the global glacial maxima within the glacial–interglacial cycles (Hughes and Gibbard, 2018). This corresponds to the classic asymmetrical pattern of ice buildup in 100 ka glacial–interglacial cycles (Broecker and van Donk, 1970). The greater magnitude of the second major global ice advance is reflected in the larger dust peak associated with it compared with the first major advance, such as when comparing MIS 4 and 2 in the last glacial–interglacial cycle (Fig. 3). However, Hughes and Gibbard (2018) identified differences between glacial–interglacial cycles, with some exhibiting different patterns. For example, in MIS 10 and 8, the first phase of glacial buildup corresponded to the largest dust peaks, and the later global glacial maxima was associated with much smaller dust peaks in Antarctic ice-core records (Fig. 4). Other anomalies are also evident when considering the pattern of glaciations from the perspective of the marine isotope record. For example, some major stadials occur within interglacial complexes (such as MIS 7d) (Ruddiman and McIntyre, 1982). These represent "missing glaciations" in the sense that they are rarely recorded on land. However, it is important to understand that glaciers would have been more extensive than today in most areas of the world in all cold intervals of major glacial–interglacial cycles. The evidence that glaciations are "missing" simply arises because their spatial coverage has been overridden by later, more extensive glaciations.

We test the hypothesis that the cold phases of some glacial–interglacial cycles were characterized by less extensive glaciations than others. To do this, we examine in this article the evidence for Middle Pleistocene glaciations after MIS 16, which marked the onset of the largest 100 ka glacial cycles (Hughes and Gibbard, 2018). We focus on MIS 8, 10, and 14 together with other intermediate intervals (MIS 7d, 13b, and 15b) and test whether the concept of "missing glaciations" is valid for these cold intervals. We aim to explore reasons for the differences in the terrestrial glacial records between and within glacial–interglacial cycles by examining the wider environmental imprint of global glaciations alongside the drivers of global climate change.

https://doi.org/10.1017/qua.2019.76 Published online by Cambridge University Press

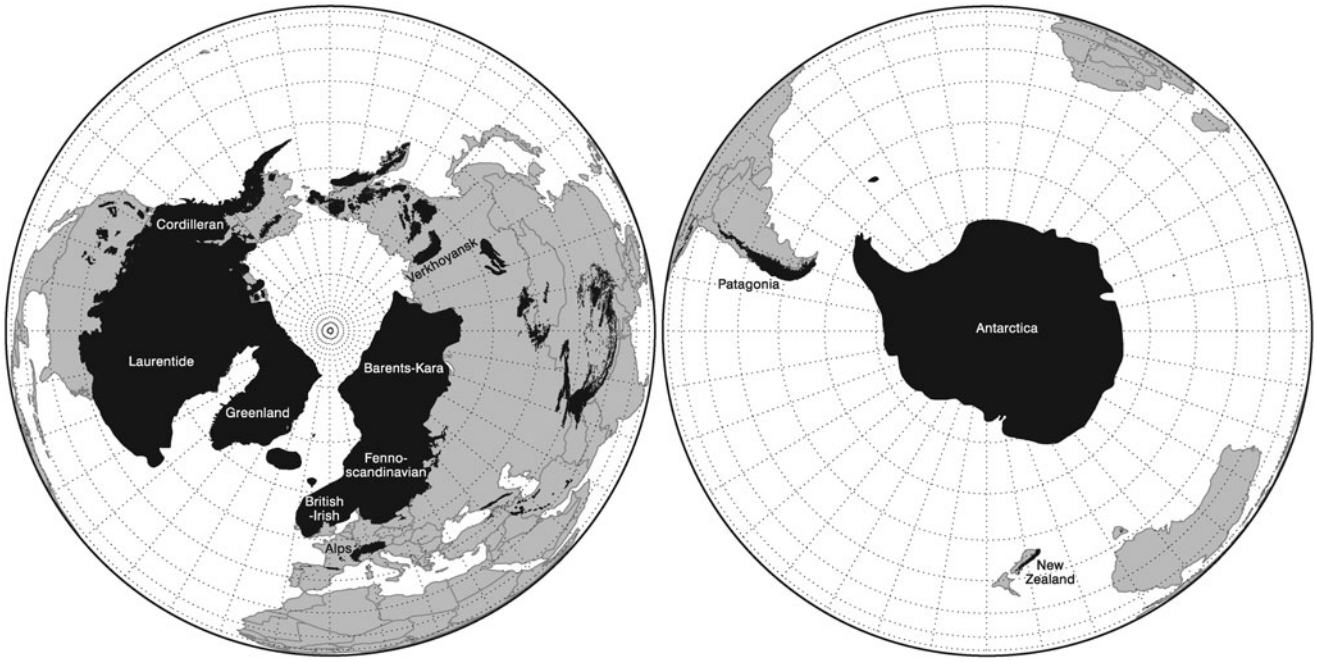

Figure 2. Maximum extent of glaciation around the globe during the last glacial–interglacial cycle (Weichselian, Wisconsinan, and Valdaian Stages and equivalents). The extents depicted here are diachronous with ice masses reaching their maximum positions at different times. The extents would have also varied in different glacial–interglacial cycles, although the general differences in extents of the largest continental ice masses is typical of the relative contributions of ice on Earth by the major regional ice masses. This figure illustrates the relative sizes of the ice masses and their spatial distributions and highlights the spatial dominance of the ice masses in the Northern Hemisphere. Redrawn and adapted from Ehlers and Gibbard (2007) and Hughes et al. (2013).

METHODOLOGICAL APPROACH

Glacial records

The geologic and geomorphological evidence for glaciation is based on published papers from sites around the world. This evidence includes large compilations and reviews such as those in Ehlers et al. (2011a, 2011b) and many other sources, including many new data sets from the last few years. A key focus is on dated records, which for the Middle Pleistocene glacial record are dominated by cosmogenic exposure, optically stimulated luminescence (OSL), and uranium-series dating.

Indirect records of glaciation and global climate

Marine isotope records

Marine oxygen isotope records provide the classic proxy for global ice volume (Shackleton, 1967) and underpin modelling approaches for ice sheet reconstructions through time where direct evidence of glaciation is not available (e.g., Batchelor et al., 2019). The driver of cyclic fluctuations in marine oxygen isotopes from foraminiferal tests has long been attributed to orbital forcing (Hays et al., 1976), and this provides the time frame to which the marine isotope record is tuned (Imbrie et al., 1984; Ruddiman et al., 1989; Lisiecki and Raymo, 2005; Fig. 4). However, the marine oxygen isotope record is not a pure record of global ice volume but is a record of both global ice volume and deep-ocean temperature (Spratt and Lisiecki, 2016). Furthermore, as noted earlier, changes in the Laurentide Ice Sheet through glacial–interglacial cycles dominate the global ice volume component of the marine isotope signal due to its large size relative to other ice masses on Earth (Fig. 2). Consequently, the marine isotope record is not representative of the spatial complexity of global glaciations (Hughes et al., 2013).

Sea-level records

Global ice volume is closely intertwined with global sea levels, and the magnitude of glaciations is reflected in sea-level changes. Global sea levels through the last 800 ka were assessed using the data of Spratt and Lisiecki (2016) (Fig. 4). In their paper, Spratt and Lisiecki (2016) analysed seven Late Pleistocene sea-level records for the interval 0–430 ka and five for the interval 0–798 ka that have converted the oxygen isotope content of the calcite tests of foraminifera ($\delta^{18}O_c$) to sea level. The seven records included an inverse ice volume model (Bintanja et al., 2005), Pacific benthic $\delta^{18}O$ of seawater ($\delta^{18}O_{sw}$) (Elderfield et al., 2012), a global stack of planktonic $\delta^{18}O_{sw}$ (Shakun et al., 2015), relative sea level from the Mediterranean (Rohling et al., 2014), Atlantic benthic $\delta^{18}O_{sw}$ (Sosdian and Rosenthal, 2009), $\delta^{18}O_c$ regression (Waelbroeck et al., 2002), and a relative sea level from the Red Sea (Rohling et al., 2009). The longer record (used in this paper) for the interval 0–798 ka excluded the $\delta^{18}O_c$ regression (Waelbroeck et al., 2002) and the relative

https://doi.org/10.1017/qua.2019.76 Published online by Cambridge University Press

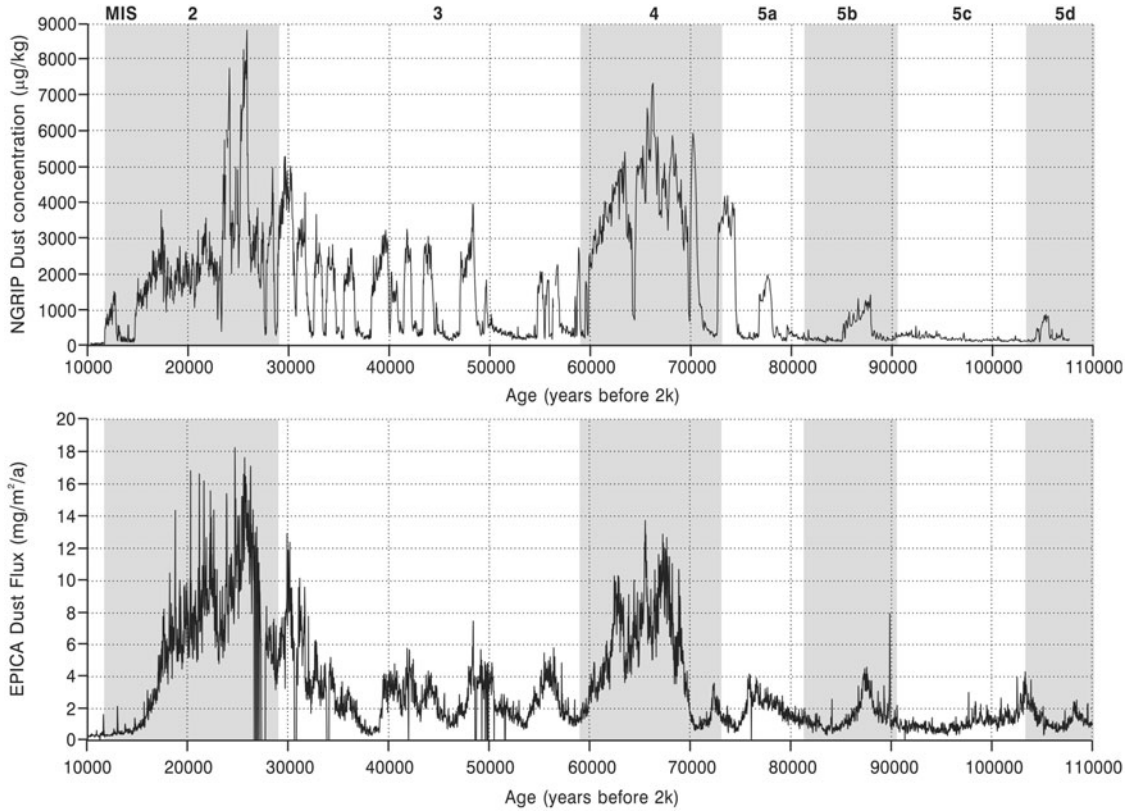

Figure 3. The dust records from Greenland (NGRIP) and Antarctica (EPICA) ice cores for the last glaciation in MIS 5d-2. The top diagram shows the dust concentration (Ruth et al., 2007) record from the NGRIP core (on the GICC05 age model). The bottom diagram shows dust flux (Lambert et al., 2012) from EPICA, Antarctica (on the EDC3 age model). The grey shaded bars represent the cold intervals (from left to right) of MIS 2, 4, 5b and 5d. The records show a strong correlation in dust records between Greenland and Antarctica, and this supports the assertion that dust records in either polar hemisphere reflect the state of the global hydrological cycle and the global atmosphere. This observation provides the template for interpreting earlier glaciations, with drier and dustier atmosphere directly related to increasing global ice coverage. This interhemispheric comparability is important, because beyond the last interglacial, studies must currently rely on the Antarctic ice-core records. Adapted from Hughes and Gibbard (2015).

sea level from the Red Sea (Rohling et al., 2009) (see Spratt and Lisiecki, 2016, Table 1).

Hughes and Gibbard (2018) analysed sea-level changes through glacial–interglacial cycles using the data of Shakun et al. (2015), who used planktonic $\delta^{18}O_{sw}$ to correct the $\delta^{18}O$ stack for non–ice volume effects. However, in their analysis of global sea-level change through glacial–interglacial cycles, Spratt and Lisiecki (2016) noted that because the surface ocean is affected by greater hydrological variability and characterises a smaller ocean volume than the deep ocean, planktonic $\delta^{18}O_{sw}$ may differ more from ice volume changes than benthic data.

Sea-surface temperature records

Shakun et al. (2015) exploited the temperature component of planktonic $\delta^{18}O$ records from 49 cores around the globe to calculate a stacked record of global sea-surface temperatures (SSTs) (Fig. 4). This now enables insights into global shifts in both climate and ice volume during glacial–interglacial cycles. This is significant, because it avoids the Laurentide problem, wherein global ice volumes are dominated by a single regional ice mass. While ice sheets do affect SSTs at the regional scale, global SSTs between different oceans are much less likely to be dominated by regional ice dynamics.

While the surface ocean is undoubtedly subject to greater hydrological variability (see Spratt and Lisiecki, 2016) and surface atmospheric processes, this is useful for gauging the state of the Earth's ocean–atmosphere interface. At individual scales, SST records are likely to be quite variable, but when combined, the stack of 49 cores used by Shakun et al. (2015) from sites located at 0–60°N and 0–60°S in the Pacific, Atlantic, and Indian Oceans does provide a global summary of the state of the ocean–atmosphere interface through glacial–interglacial cycles.

Ice-core records

Dust content in polar ice cores can provide insights into the state of the global atmosphere through time, and this was used by Lambert et al. (2008, 2012) to assess dust flux over Antarctica during multiple glacial–interglacial cycles. Hughes and Gibbard (2015; 2018) argued that peaks in

https://doi.org/10.1017/qua.2019.76 Published online by Cambridge University Press

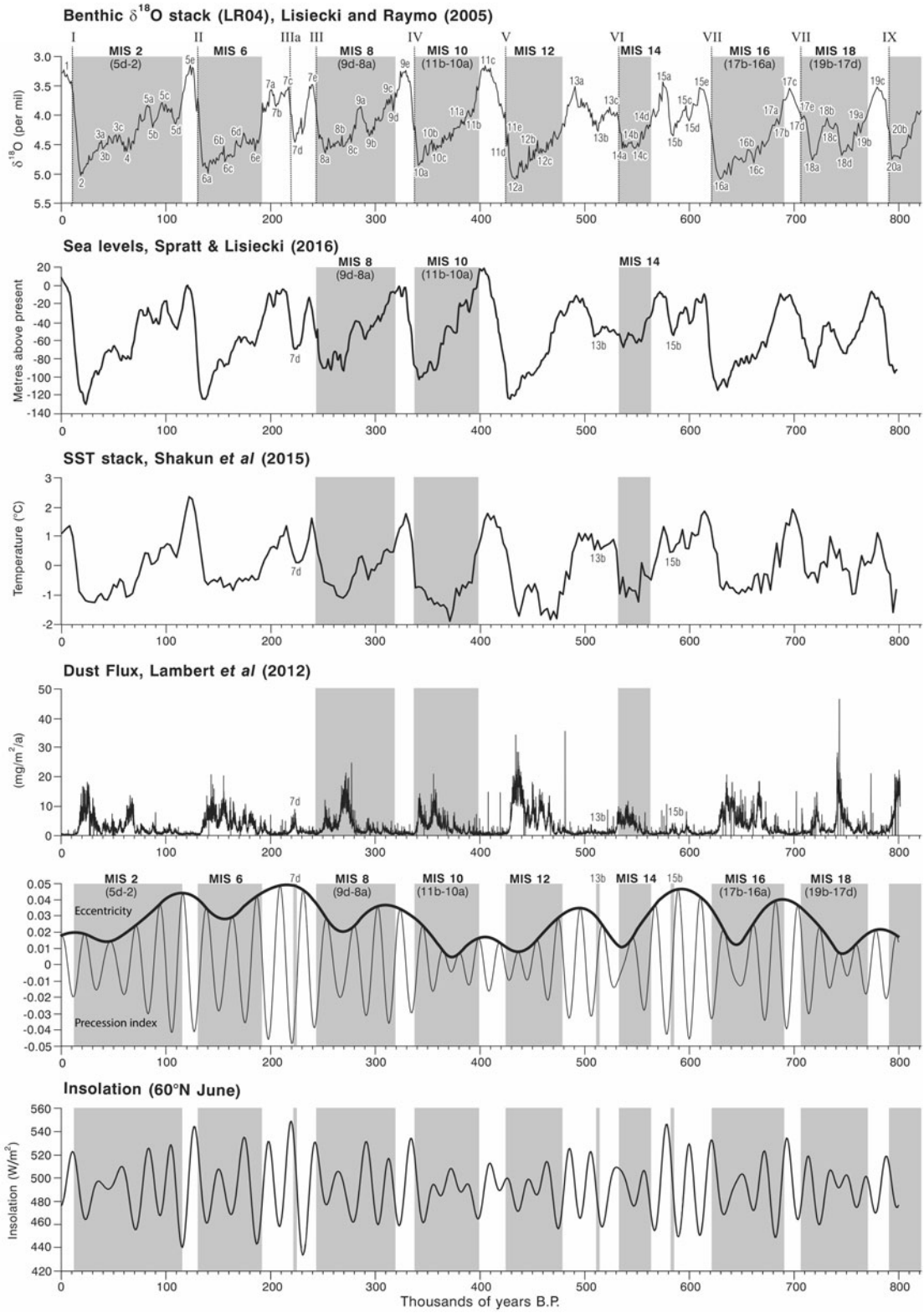

Figure 4. Graphs showing link between the structure of glacial–interglacial cycles indicated in the global benthic stack of Lisiecki and Raymo (2005), global sea levels extracted from a global stack of sea-level records (from Spratt and Lisiecki, 2016), global sea-surface temperatures (SSTs) from 49 paired SST-planktonic $\delta^{18}O$ records (Shakun et al., 2015), and dust flux from the EPICA Dome C ice-core record (Lambert et al., 2012). The Roman numerals (I, II, III, IV, etc.) over the global benthic stack indicate the positions of the respective glacial terminations. The lower two graphs illustrate solar parameters for the last 800 ka. The second from bottom graph shows the precession index and the eccentricity index from Berger and Loutre (1991) and Berger (1992). The precession index (climatological precession parameter: e sin ω; values from −1 to + 1) is an indicator of the amplitude of the seasonal cycle with a move towards autumn/winter perihelion at peaks and towards an earlier spring/summer perihelion at troughs and is determined by the variations in eccentricity (dimensionless value between 0 and 1). The bottom graph shows June insolation data at 60°N (Berger and Loutre, 1991; Berger, 1992).

https://doi.org/10.1017/qua.2019.76 Published online by Cambridge University Press

Table 1. Sea-level estimates from the global stack of Spratt and Lisiecki (2016) in order of magnitude. These values are obtained from the long stack (0–798 ka) of five sea-level reconstructions. The marine isotope stages listed represent cold-climate intervals within glacial–interglacial cycles.

	MIS	Global sea-level minima (m) in descending order of magnitude
	2	−130
	6	−124.5
	12	−124.4
	16	−114.62
"Missing	10	−102.83
glaciations"	8	−93.27
	7d[a]	−69.51
	14	−67.39
	13b[a]	−55.45
	15b[a]	−54.40

[a]MIS 15b, 13b, and 7d are stadials within interglacials.

Antarctic dust in glacial–interglacial cycles corresponded to global ice buildup in both hemispheres, and this was used as an indirect indicator of global glacial behaviour in glacial–interglacial cycles. This argument was largely built on observations from the last glacial–interglacial cycle, in which large ice buildup in MIS 4 and 2, for example, was associated with peaks in dust not only in Greenland but also in Antarctica (Hughes and Gibbard, 2015; Fig. 3).

Given that the Greenland ice-core records only span from the last interglacial, Antarctic records must be relied upon for earlier glacial–interglacial cycles. Dust flux over Antarctica has a close correlation with temperature as climate becomes colder (Lambert et al., 2008). Comparison of Antarctic ice-core dust records with loess/palaeosol sequences from the Chinese Loess Plateau (Kukla et al., 1994) confirms the synchroneity of global changes in atmospheric dust load (Lambert et al., 2008). However, being a Southern Hemisphere record, comparisons of dust peak magnitudes cannot necessarily be transferred to interpreting the size of global ice volume, only the temporal pattern and possibly the hemispheric distribution of ice masses. Nevertheless, Antarctic dust records are broadly representative of the global hydrological cycle, with increasing dust indicating a cooler and drier global atmosphere that is directly associated with the extent of global glaciations.

Dust records may be a better reflection of global ice spatial coverage on land than marine isotope records, which partially reflect ice volume. This is because increased ice coverage over land surfaces causes increased aridity in peripheral areas due to the effects of ice masses on regional climate (Manabe and Broccoli, 1985). This occurs today where strong anticyclones form over modern ice sheets (Hobbs, 1945). The aridity effects would have been compounded during the Pleistocene cold phases due to the effects of not just low precipitation but also low atmospheric CO_2 on plant growth (Claquin et al., 2003).

Drivers of global glaciations: solar forcing and CO_2

We examine the patterns of Earth-orbital changes and glacial–interglacial cycles to see whether there is any relationship between "missing glaciations" and orbital forcing. Solar radiation is important when considering glaciations, because it controls the energy receipt to the Earth and thereby impacts glacial mass balance, especially ablation. In their synthesis of the last 10 glacial–interglacial cycles, Hughes and Gibbard (2018) showed that variations in solar radiation in the Northern Hemisphere were responsible for ~50%–60% of variations in global ice volume. For example, troughs in solar radiation at the end of interglacials and beginning of subsequent cold stages are thought to be associated with rapid glacial advances in the continental interiors and high- and mid-latitude mountains (Hughes and Gibbard, 2018). This hypothesis is tested further here by quantifying the magnitude of solar peak–trough changes at the transition between interglacial and glacial intervals (Fig. 4). This was done by calculating a value for solar-trough magnitude (STM), which describes the trough magnitude and time span at 60° N. This is derived by taking the median (50th percentile) solar radiation value (W/m^2) between the trough and the preceding peak (s_m) and dividing this by the trough time span (s_t) (defined by the time in years between the trough and the preceding peak), then inverting this value:

$$STM = 1/(s_m/s_t)$$

We also examine the orbital record further by isolating the effects of orbital parameters such as eccentricity, obliquity, and precession on global glacial dynamics within and between glacial–interglacial cycles. Eccentricity controls the shape of the Earth's orbit around the sun and directly affects the influence of variations of precession (i.e., on the timing of perihelion and aphelion) and the seasonal distribution of solar radiation. The interaction of eccentricity with precession is indicated in the precession index (Fig. 4). In addition to solar radiation, Ganopolski et al. (2016) highlighted the importance of CO_2 in glacial inception. They identified points in time when low CO_2 corresponded with low insolation as potential triggers for global ice buildup. This hypothesis implies that low insolation alone cannot explain global glacial inception. Instead, it is the combination of insolation forcing with atmospheric CO_2 concentrations that drives glacial inceptions. Over the longer term, declining atmospheric CO_2 through the Quaternary has been linked to the removal of weathered regolith by glacial erosion over North America and Europe (Clark and Pollard, 1998). This causal mechanism may partly explain the transition to the large-magnitude 100 ka glacial–interglacial cycles at the Early–Middle Pleistocene transition (Clark and Pollard, 1998; Ganopolski and Calov, 2011; Tabor and Poulsen, 2016; Willeit et al., 2019).

Terminology

There are three ways to define glacial–interglacial cycles (Hughes and Gibbard, 2018):

https://doi.org/10.1017/qua.2019.76 Published online by Cambridge University Press

1. the periods between glacial terminations;
2. the periods of cold phases defined by global SSTs within glacial–interglacial cycles (cf. Shakun et al., 2015), and;
3. the span of traditional subdivision of cold intervals based on marine isotope stages and substages (Railsback et al., 2015).

The term *cold stage* refers to climatostratigraphic/chronostratigraphic units such as the Weichselian or Wisconsinan in Europe or North America, respectively, which are equivalent to MIS 5d-2. This is complicated by the fact that some cold stages in this definition span multiple glacial–interglacial cycles, such as the Saalian and Wolstonian Stages in continental Europe and the British Isles, respectively. Marine oxygen isotope stages are distinct from chronostratigraphic cold stages and sometimes multiple marine isotope stages make up a single cold stage in the strict sense. For example, the Weichselian/Wisconsinan stages include MIS 5d-2 and also the early part of MIS 1. A global correlation table based on the chart of Cohen and Gibbard (2011) is provided in Figure 1 to aid cross-comparison between marine isotope events and terrestrial chronostratigraphy.

THE "MISSING GLACIATIONS"

MIS 8 (Middle Saalian and equivalents)

MIS 8 occurs within a larger glacial–interglacial cycle between termination IV and III (Fig. 4). Overall, this was a relatively weak glacial–interglacial cycle. The glacial inception occurred at the boundary of MIS 9d/e at ca. 320 ka. MIS 8 has a weak signal of global glaciation in many records, particularly benthic $\delta^{18}O$ (Lang and Wolff, 2011), and is second only to MIS 14 in terms of maximum $\delta^{18}O$ values for the last 10 glacial–interglacial cycles (Fig. 4). At −93.27 m, MIS 8 had the highest sea levels of the last six 100 ka glaciations (Table 1). The lowest sea levels do not coincide with the trough in benthic $\delta^{18}O$ values (at 252 ka) but occurred ca. 18 ka earlier at 270 ka in MIS 8c (Fig. 4). A strong interstadial (MIS 9a) separates two marine isotope troughs (MIS 8a-c and 9b).

The solar-trough magnitude at the beginning of this glacial–interglacial cycle was one of the weakest of the last seven glacial–interglacial cycles (Table 2). This is likely to have resulted in a weak glacial inception and explains the weak stadial conditions in MIS 9d, which is characterised by relatively minor excursions in benthic and planktonic isotope values and moderate influence of subpolar water masses (Roucoux et al., 2006). In their core from the Iberian margin, Roucoux et al. (2006) argued that the pollen evidence suggests a less arid and cold climate than during other stadial intervals, when steppe was more abundant and temperatures offshore were lower.

Dust flux over Antarctica for MIS 8 reached some of the highest and sustained levels of the last million years, reaching values comparable with MIS 6, yet more sustained, and greater than MIS 5d-2 (Fig. 4). Significantly, the dust peak in Antarctica does not coincide with the largest marine isotope trough of MIS 8a. Instead, it occurs earlier at ca. 272 ka in MIS 8c, coinciding with the lowest sea levels. Hughes and Gibbard (2018) noted that the first dust peak also coincides with the lowest CO_2 levels (Ganopolski et al., 2016) and the coldest global SSTs of this glacial period (Shakun et al., 2015). Pollen records from a marine core on the Iberian margin match these patterns and show the most extreme glacial conditions of MIS 8 occurred during the early part, followed by an interval of warmer conditions and tree population expansion after 263 ka (Roucoux et al., 2006). This suggests that the configuration of controls of global climate (including insolation, atmospheric composition, land cover, sea ice, and the ice sheets themselves) were different in MIS 8 from other glaciations, such as MIS 6 and 5d-2. In these later glaciations, the global ice maxima and associated cold and dry indicators occurred towards the end of the glacial–interglacial cycle.

Examination of the record of glaciation during this period (i.e., ca. 320–243 ka) repeatedly shows that evidence of glaciation is poorly represented throughout much of the world's glaciated regions. In northern Europe, the traces of glaciation that can be reliably attributed to this time are rare. The few deposits that have been identified in northwest Europe are mainly based on isolated numerical age determinations, especially OSL or amino acid racemisation analyses of adjacent sediments or their contained fossil materials. For example, the most often quoted example is that reported by Beets et al. (2005) suggesting that pre-Late Saalian (i.e., Middle Saalian; MIS 8) till occurs in the North Sea basin based on geophysical, micropalaeontological, and amino acid age evidence. While there is no question that till occurs at the site, there remains scepticism about the age attribution among Dutch workers who generally attribute these deposits to the Late Saalian (MIS 6; Cohen, K.M., personal communication, 2017). Despite other possible MIS 8 records from other circum–North Sea localities (e.g., White et al., 2010, 2017; Davies et al., 2012; Bridgland et al., 2014; Roskosch et al., 2015) all of these remain equally equivocal. In contrast, as in the Netherlands, recent dating evidence from eastern England has confirmed that a major glaciation did occur in MIS 6 (Evans et al., 2019) confirming the Wolstonian (= Saalian) age of a glaciation that reached into the Fenland basin in eastern England (Gibbard et al., 2018). The lack of a regional till sheet and consistent biostratigraphy appears to support the view that glacial ice did not extend into the central western European area and the central and southern North Sea basin (Huuse, M. personal communication, 2017) during MIS 8. However, there is evidence for Middle Saalian glaciation that reached the continental shelf edge off Norway, Svalbard, and Scotland, according to Sejrup et al. (2000, 2005). In southern Jæren in southwestern Norway, this glaciation is represented by the Vigrestad Till (glacial F: Sejrup et al., 2000). In Denmark, westward-flowing meltwater streams deposited sand and gravels over much of central and southern Jylland. These streams derive from the first Saalian ice advance that occurred during MIS 8, which deposited the Treldenæs Till (Houmark-Nielsen, 2004, 2011). This Norwegian Saale advance invaded Denmark from the north,

https://doi.org/10.1017/qua.2019.76 Published online by Cambridge University Press

Table 2. Solar radiation peak-trough amplitude at 60°N early in cold stages or at the end of preceding interglacials. Solar-trough magnitude describes the peak-trough magnitude and time span. This is derived by taking the median value between the preceding solar peak and subsequent trough and scaling (dividing) this by the peak to trough time span, then inverting this calculated value. Solar radiation data are derived from Berger and Loutre (1991) and Berger (1992). Marine Isotope Stages are listed in descending order of solar-trough magnitude. The Marine Isotope Stages associated with the "Missing Glaciations" are shown separately at the bottom of the table.

	Marine Isotope Stage (cold stage in bold)	Preceding peak[a]	Age (ka)	Trough[a]	Age (ka)	Amplitude change	Median peak-trough[a]	Peak-trough time span (ka)	Solar-trough magnitude
	MIS 7/**6**	531.96	198	443.00	187	88.96	487.48	11	0.0226
	MIS 13/**12**	525.83	486	456.22	475	69.61	491.03	11	0.0224
	MIS 17/**16**	534.77	693	448.99	682	85.78	491.88	11	0.0224
	MIS 6e/**5d-2**	544.69	127	440.20	116	104.49	492.45	11	0.0223
"Missing glaciations"	MIS 15/**14**	546.62	579	454.66	567	91.96	500.64	12	0.0240
	MIS 9/**8**	517.25	313	459.83	303	57.42	488.54	10	0.0205
	MIS 11/**10**	508.45	373	484.84	363	23.61	496.65	10	0.0201

[a]Insolation (W/m^2).

probably terminating south of the Danish–German border in Schleswig-Holstein (Houmark-Nielsen, 2011).

In northwest Europe, Toucanne et al. (2009a) noted that Fleuve Manche fluvial discharge through the English Channel was significantly less during MIS 8 than during MIS 6 and 2 (indicated by lower mass accumulation rates [MAR] in Fig. 5). This is consistent with smaller ice masses in northern Europe and the Alps, the meltwater from which drained into this river system in MIS 8. Furthermore, in the northeast Atlantic Ocean at Ocean Drilling Programme (ODP) Site 980 (55° 29′N, 14°42′W) summer SSTs were generally warmer in MIS 8 than in MIS 6 and 2 (McManus et al., 1999). However, oscillations in SSTs were large, with minimum temperatures on a par with MIS 6 and 2. In fact, the quantities of ice-rafted debris (IRD) in the northeast Atlantic during MIS 8 and 10 were significantly larger than in MIS 6 and 2 (McManus et al., 1999). This was related to high-amplitude millennial-scale climate change, which is also reflected in terrestrial vegetation records in Europe (Fletcher et al., 2013). The muted signal in the Fleuve Manche discharge in contrast to a strong signal in the IRD in the northeast Atlantic suggests the configuration of ice masses in this region differed between glacial–interglacial cycles.

In Poland, the Krznanian glaciations are correlated with MIS 8 (Lindner and Marks, 1999). According to Marks (2011), Poland was invaded by ice sheets derived from Scandinavia during the Liwiecian, Krznanian, and Odranian intervals within the Saalian Stage. The limit of the Odranian glaciation can be mapped at the modern land surface, whereas the Liwiecian and Krznanian are buried by younger deposits. During the latter, an ice sheet advanced into eastern Poland, reaching as far south as the northern foreland of the South Polish Uplands, and it probably also approached the Silesian Upland. This advance may have also crossed the Baltic states, Latvia and Lithuania, and presumably parts of Belarus.

In neighbouring European Russia, glaciation during this period seems to have been markedly less extensive than during the Late Saalian–equivalent Dniepr and Moscow glaciations (MIS 6) (Velichko et al., 2011; Fig. 1). However, east of the Urals it is represented by the substantial till of the Samarovo glaciation, the deposits of which form the maximum glacial drift boundary in western Siberia. This major glaciation is correlated with MIS 8 (Fig. 6) based on regional stratigraphic successions (Astakhov et al., 2016).

While the limit is based on boreholes and rare natural sections in the west Siberian Plain, in the central Siberian Uplands the boundary has been mapped based on chains of push moraines and occasionally where it overlies interglacial fluvial deposits in buried valleys (Rudenko et al., 1984; Astakhov, 2011). In the western Siberian Plain and the central Siberian Plateau, the Samarovo glaciation was consistently much more extensive than the later Taz glaciation, which is thought to date from later in the Saalian Stage in MIS 6 (Astakhov et al., 2016). Given the scale of the land areas involved, these Siberian ice masses would have been major contributors to global ice volume.

In the mountains of central and southern Europe, evidence of glaciation in MIS 8 has been recognised in Iberia (Fernández Mosquera et al., 2000; Vidal Romaní et al., 2015), Italy (Giraudi and Giaccio, 2017), and the Alps (Preusser et al., 2011). In Baden-Württemberg and Bavaria, southern Germany, the multiphased Riss glaciation is provisionally correlated with MIS 10–6 (Doppler et al., 2011). In the Balkans, there is also some evidence of MIS 8 glaciation (Hughes et al., 2011). In the Italian Apennines, Giraudi et al. (2011) reported that there was no evidence for glaciation in MIS 8, unlike for other Middle Pleistocene glaciations. However, later work in the same basin revealed evidence of two glaciations between 350 and 130 ka, and these were correlated with MIS 8 and 6, although the relative sizes of these two glaciations was not established (Giraudi and Giaccio, 2017).

In North America, evidence of glaciation attributed to the MIS 8 interval is equally elusive. In northwest Canada and eastern Alaska, where till and associated deposits of the Reid glaciation are frequent (Duk-Rodkin et al., 2004; Duk-

https://doi.org/10.1017/qua.2019.76 Published online by Cambridge University Press

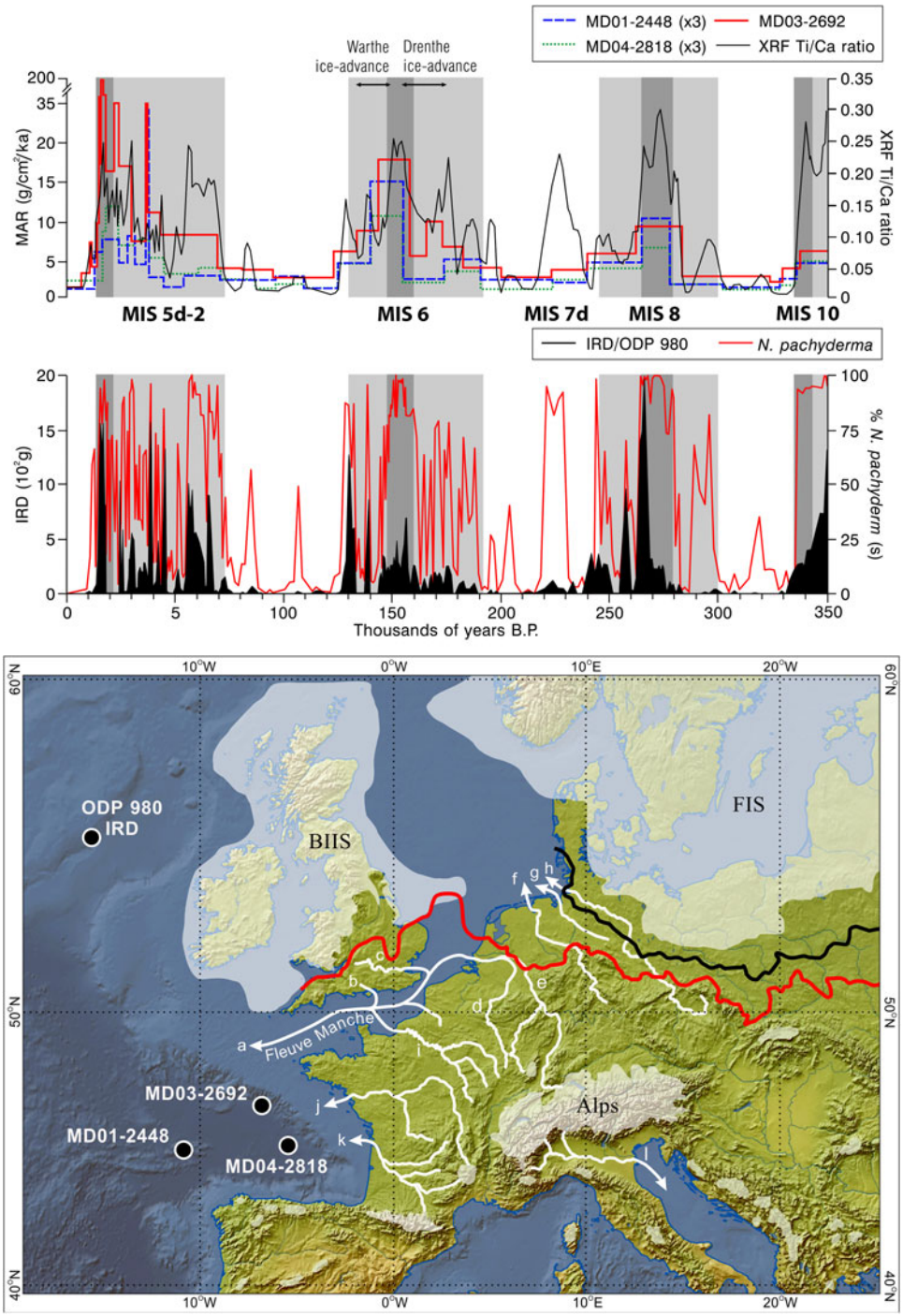

Figure 5. (color online) Top, mass accumulation rates (MAR) in marine sediment records in the Bay of Biscay, northeast Atlantic Ocean (from Toucanne et al., 2009a). The MAR graph is from sites MD03-2692 (46°49.72′N, 9°30.97′W), MD01-2448, and MD04-2818. Lower MAR in MIS 10 and 8 compared with MIS 5d-2 and 6 are interpreted as indicating less glaciofluvial discharge, primarily through the former English Channel fluvial system (Fleuve Manche). The XRF Ti-Ca ratio reflects terrigenous sediment input, but is also associated with an ice-rafted debris (IRD) source. The IRD graph is from site ODP 980 from farther north in the northeast Atlantic Ocean (55°29′N, 14°42′W) off the British–Irish continental shelf (data from McManus et al., 1999). The bottom map shows the locations of these core sites relative to the former ice masses. The approximate positions of the Late Pleistocene ice limits for the northern ice sheets (BIIS, British–Irish Ice Sheet; FIS, Fennoscandian Ice Sheet) are given for reference in white shading together with the Late Saalian (MIS 6) ice limits shown in red/grey (Drenthe advance) and black (Warthe advance). The outlines and positions of ice masses in central and southern Europe are schematic due to scale. The white arrows and the associated lowercase letters identify the main European rivers: a, Fleuve Manche; b, Solent; c, Thames; d, Meuse; e, Rhine; f, Ems; g, Wesser; h, Elbe; i, Seine; j, Loire; k, Gironde; l, Pô. Redrawn and adapted from Toucanne et al. (2009a). (For interpretation of the references to color in this figure legend, the reader is referred to the web version of this article.)

https://doi.org/10.1017/qua.2019.76 Published online by Cambridge University Press

Figure 6. (color online) Limits of the Eurasian contiguous ice sheets during the Middle and Late Pleistocene. Adapted from information in Svendsen et al. (2004), Astakhov et al. (2016) and Hughes and Gibbard (2018). East of the Urals, the most extensive glaciation occurred in MIS 8, although evidence of this glaciation is largely absent to the west in Europe.

Rodkin and Barendregt, 2011), there is some doubt regarding the correlation of these materials to either MIS 6 or 8, or both, or in some cases younger intervals (Ward et al., 2008; for discussion see Duk-Rodkin et al., 2004; Barendregt and Duk-Rodkin, 2011). In some areas, OSL dating of glaciofluvial deposits over- and underlying till has determined the age of the Reid glaciation as MIS 6 (Demuro et al., 2012). Equivalents to the MIS 6 or 8 glaciations are almost certainly present in the Mackenzie Mountains, where as many as three tills occur beneath the Late Pleistocene Laurentide glacial deposits at the surface. On Banks Island in the Canadian Arctic, till underlying last interglacial (Sangamonian Stage) Cape Collinson glaciomarine deposits are termed the Thomsen glaciation (250 ka). These deposits are thought to mark the maximum extent of Middle Pleistocene glaciation in northwestern Canada (Duk-Rodkin et al., 2004).

Elsewhere in North America evidence is found in the Sierra Nevada, where several till units appear to date from the MIS 8–6 (303–186 ka) interval, but here the age control is insufficient to distinguish the individual events to which they relate (Gillespie and Zehfuss, 2004; Gillespie and Clark, 2011). Despite previous reports of MIS 8–age glacial deposits in Glacier National Park, the early Bull Lake Till (Richmond, 1986), it is now thought that no deposits of this age occur in this district (Fullerton et al., 2004). In Illinois, the southern margin of the Middle Pleistocene Laurentide Ice Sheet extended 150 km beyond the later Wisconsinan (MIS 5d-2) limits. Stiff and Hansel (2004) suggested that glacial deposits of MIS 8 may be present in these more extensive limits. However, Curry et al. (2011) argue that the combination of evidence from palaeosols and a range of different dating techniques (OSL, ^{10}Be, amino acid geochronology) indicate that the Illinoian glaciation is restricted to MIS 6. In Missouri, till units have been shown to predate MIS 6 using ^{10}Be burial dating, although the imprecision of this technique means that correlations for these tills can be made with MIS 8, 10, or even 12 (Rovey and Balco, 2011). In western Wisconsin, two till formations are related to the "Illinoian glaciation" (s.l.), which in this region is dated to 300–130 ka (Syverson and Colgan, 2004, 2011). These units, derived from the Superior province, extend beyond the Wisconsinan ice-maximum limits. However, it is not known to which marine isotope stage they relate. Patchy deposits of similar age occur in southern Wisconsin and northern Illinois (Syverson and Colgan, 2004, 2011), but again may relate to MIS 6.

In South America, evidence from the tropics is once again rather limited, although there is strong evidence of MIS 8 glaciation in Patagonia. Here, ^{10}Be concentrations in outwash cobbles indicate a major glacial advance at ca. 270-260 ka, within MIS 8. This is close in time to the most pronounced dust peak in MIS 8 in Antarctic ice cores (Hein et al., 2009, 2017). Significantly, Hein et al. (2009, 2017) found that exposure ages from dated outwash terraces are 70–100 ka older than the associated moraines. Based on geomorphological observations, the authors suggested that this difference can be explained by exhumation of moraine boulders.

https://doi.org/10.1017/qua.2019.76 Published online by Cambridge University Press

Elsewhere in the Southern Hemisphere, the large moraines occurring at the mouths of valleys and cirque basins in western Tasmania were thought to have marked the last glaciation (MIS 2) limits, such as in the West Coast Range (Lewis, 1945; Colhoun, 1985). However, recent exposure dating has demonstrated that this is incorrect and that some of these moraines were formed during the Middle Pleistocene (Barrows et al., 2002; Kiernan et al., 2010). In their review, Colhoun and Barrows (2011, p. 1042) stated that the Hamilton Moraine, west of Lake Margaret, formed during MIS 8.

In New Zealand, weathered till correlated with MIS 8 (Rattenbury et al., 2006), near Edwards Pass between the Waiau and Clarence valleys, lies about 20 km downvalley from the MIS 2 termini. However, a geochronological basis for this correlation is lacking, and for most glaciations predating MIS 6, correlations with the marine isotope record are made using relative and biostratigraphic criteria (Barrell, 2011). With respect to the Middle Pleistocene glaciations in New Zealand, only MIS 6 glaciations have been confirmed by dating (e.g., Rother et al., 2010).

Overall, glaciation associated with MIS 8 is rarely found or at least not conclusively confirmed in most regions. Glacial extents in MIS 6 were consistently larger, and this is supported by a much wider body of evidence. Major exceptions to this occur in Russia east of the Urals and in Patagonia.

MIS 10 (Early Saalian and equivalents)

Superficially, the marine oxygen isotope sequence for MIS 10 resembles those of other major glaciations, with a structure similar to MIS 12, but less severe. For example, global sea levels were −102.83 m compared with −124.4 m for MIS 12, yet more than 9 m lower than in MIS 8 (Table 1). However, the dust record from Antarctica indicates two major dust peaks, one at ca. 342–341 ka corresponding with the "glacial maximum" indicated in the marine isotope record (MIS 10a) and another even larger dust peak earlier in the glacial–interglacial cycle at ca. 355 ka (Fig. 4). The largest dust peak occurs in substage MIS 10b and corresponds with an early sea-level trough of −92.82 at 356 ka. This dust peak and low sea-level stand is preceded by the coldest part of MIS 10 (at the start of MIS 10c) recorded in global SSTs (Shakun et al., 2015; Fig. 4) and the lowest atmospheric CO_2 levels of the glacial–interglacial cycle (Hughes and Gibbard, 2018).

Solar radiation in the Northern Hemisphere was lowest late in the glacial–interglacial cycle, close in time to the glacial maximum indicated in the marine isotope record (Fig. 4). Before this insolation was relatively high and sustained at >480 W/m^2 with only minor troughs earlier in the glacial–interglacial cycle, except for a more significant trough at the MIS 11c/11b boundary, which marks the beginning of the glacial–interglacial cycle. The solar-trough magnitude at the preceding interglacial–glacial transition was the weakest of all the last seven glacial–interglacial cycles (Table 2).

As for MIS 9d-8a, glacial deposits dating from the interval represented by MIS 11b-10a (ca. 400–337 ka) are very poorly represented in northwest Europe. In the southern and central North Sea region there is no record, although Norwegian and Svalbard ice extended to the shelf margin as indicated in offshore accumulations, according to Sejrup et al. (2005) and confirmed by IRD. The glaciation is represented by an unnamed till underlying the Varhaug marine sediments in the Hobberstad borehole (Sejrup et al., 2000). In North Sea surveys, Graham (2007) mapped ice-stream bed structures within the Coal Pit Formation in the Witch Ground basin. Although the age correlation in this basin is not ideal, the features suggest shelf glaciation between MIS 10 and 6 (Graham et al., 2011). However, as in MIS 8, the ice was most probably markedly more limited in extent. Scandinavian and British ice masses were almost certainly not confluent across the North Sea basin during these phases (Toucanne et al., 2009a, 2009b). As with the MIS 8 evidence, there are some isolated age determinations that did hint at possible MIS 10–age glacial advances (e.g., Scourse et al., 1999) in the Nar Valley area of Norfolk in eastern England. However, these determinations have been questioned and more recently rejected (Gibbard and Clark, 2011). While ice masses over northwest Europe were restricted in MIS 10, there was nevertheless significant ice rafting in the North Atlantic reaching as far south as the Bay of Biscay (e.g., McManus et al., 1999; Toucanne et al., 2009a; Fig. 5).

Elsewhere in Europe, the evidence for MIS 10–equivalent age glaciation is fragmentary. In the Alps, glaciation may have happened, but the evidence has not been dated (Van Husen and Reitner, 2011). Poland once again preserves a record of post-Holsteinian (Mazovian) interglacial stage glaciation that has been correlated with MIS 10. This Liviecian glaciation was the first glacial episode of the Saalian Stage (s.s.) and preceded the Zbójnian interglacial. During this event, the ice sheet reached central Poland (Lindner and Marks, 1999).

In Russia, glacial deposits that have been reliably attributed to MIS 10 are very rare. However, Astakhov (2004, 2011) suggested that a sequence found in Siberia possibly represents a transition between MIS 10 and 9 where deep-marine sedimentation resulting from isostatic loading from the previous phase of glaciation is found. This dating is based on electron spin resonance and green stimulated luminescence ages of 400–300 ka. Similar ages have been reported for marine deposits from a few localities on the Taymyr Peninsula (Bolshiyanov et al., 1998). If this interpretation is correct, then it implies the development of a substantial ice cap over northern Siberia in MIS 10.

In North America, there is evidence of several glacial advances during the Middle Pleistocene. However, the age of these is unclear. For example, in Pennsylvania Braun et al. (2011) correlated the early Middle Pleistocene glaciation with the pre-Illinoian D (MIS 16) and a later advance with the pre-Illinoian A or B (MIS 10 or 12; i.e., Early Saalian and Elsterian) or Illinoian (Late Saalian: MIS 6) (using the terminology of Richmond and Fullerton, 1986). Very few sites have been directly dated. An exception is in the Stikine Valley in northwestern British Columbia, where glacial and glaciofluvial deposits underlie basalts dated by K-Ar to 330 ± 30 ka in the Tathitan Canyon and by Ar-Ar to 300 ± 100 ka in

https://doi.org/10.1017/qua.2019.76 Published online by Cambridge University Press

the nearby Stikine Canyon (Spooner et al., 1996; Duk-Rodkin and Barendregt, 2011). A phase of glacier advance and retreat associated with underlying deposits is argued to have occurred between 330–360 ka, during MIS 10, immediately prior to the emplacement of the basalts (Spooner et al. 1996).

In the Southern Hemisphere there is little evidence in the glacial record of MIS 10 glaciation. However, in the western Arthur Range of southwestern Tasmania, cosmogenic exposure dating suggests that moraines were formed by glaciations in MIS 6 and 10 but not in MIS 8 (Kiernan et al., 2010). The authors do acknowledge that the MIS 10 age may be an overestimate if the erosion rates are too high, and in that case, the moraines would be MIS 8 in age.

MIS 14

MIS 14 was characterised by limited global ice extent. The signal of climatic/environmental change is particularly weak in a range of records, marine and terrestrial, leading Lang and Wolff (2011, p. 375) to argue that "it is sufficiently weak that one could question its designation as a glacial." In the marine isotope record, the maximum $\delta^{18}O$ value of this cold stage was 4.55 at 548 and 536 ka, which is the lowest $\delta^{18}O$ value of all the last 10 cold stages (Fig. 4). Ice volume was the lowest of all the last 10 glacial–interglacial cycles, with global sea levels much higher than in other cold stages at −67.39 m at 537 ka (Fig. 4, Table 1). Sea levels reached −62.75 m at 550 ka and remained depressed through to MIS 13b (−55.45 m), suggesting that the definition of this glaciation spans a longer interval than just MIS 14, despite termination VI being recorded in the marine isotope record and a sharp rise in global SSTs at this time (Fig. 4). The start of MIS 14 was associated with the strongest solar-trough magnitude of the last seven glacial–interglacial cycles (Table 2). However, this was mitigated by the fact that preceding peak in solar radiation (and median peak-trough value) was the largest solar peak at the glacial inception of the last seven glacial–interglacial cycles. Despite the evidence of limited global ice extent, global SSTs during MIS 14 were as cold as during other cold stages that were characterised by much bigger glaciations (Shakun et al., 2015). The Antarctic dust signal for MIS 14 is much weaker than for any other glacial–interglacial cycles, with dust flux <12 mg/m^2/yr. A double-peak pattern is evident at ca. 540 and 530 ka, with the first peak larger than the second (Fig. 4).

There is little direct evidence of glaciation on land from MIS 14, probably because it was limited in extent compared with later glaciations. However, in the Italian Apennines a glacial advance has been dated to MIS 14 by applying $^{36}Ar/^{40}Ar$ dating to tephra deposits in a pro-glacial lacustrine sequence in the Campo Felice basin (Giraudi et al., 2011).

The glaciations that didn't make it: MIS 7d, MIS 13b, and 15b

Some intervals characterised by major excursions in the marine oxygen isotope curve do not fit the criteria for definition as glacial–interglacial cycles as set out in Hughes and Gibbard (2018). They either do not end in formally defined terminations, are insufficiently cold as recorded in proxies such as global SSTs, or have not been assigned full-stage status in the marine isotope record. In Antarctic dust records from MIS 7d, 13b, and 15b the dust flux is relatively insignificant compared with full glacial–interglacial cycles. While Antarctic dust flux cannot be directly related to global ice volumes, only patterns of change, it nevertheless suggests that these intervals did not have significant effects on the global hydrological cycle. However, MIS 7d, 13b, and 15b are each represented by high-amplitude excursions of the $\delta^{18}O$ curve in the marine isotope record, and their magnitude stands out compared with other stadials within glacial–interglacial cycles (Fig. 4).

MIS 7d is the most pronounced of the three anomalous isotopic stadials (cf. Ruddiman and McIntyre, 1982) and had a $\delta^{18}O$ value almost as high as MIS 14 in the stacked record of Lisiecki and Raymo (2005). In fact, in the sea-level stack of Spratt and Lisiecki (2016), MIS 7d has a slightly lower sea level than MIS 14, at −69.51 m (MIS 7d) versus −67.39 m (MIS 14) (Fig. 4, Table 1). For other indicators, such as Shakun et al.'s (2015) global SST stack, MIS 7d is a significant stadial, but MIS 14 is much colder. In the same record, both MIS 13b and 15b are insignificant events, yet they recorded global sea levels at −55.45 and −54.4 m, respectively, and with large isotopic excursions in the marine $\delta^{18}O$ record (Fig. 4). This suggests that these glaciations represented large regional but not global glaciation events. The very weak dust signal in the Antarctic ice-core record for MIS 15b and 13b suggests that these glaciation events were confined to the Northern Hemisphere and had little impact on the global atmosphere. MIS 7d, however, has left a much clearer mark in the Antarctic dust record (Fig. 4). In the Northern Hemisphere, very low arboreal pollen percentages in southern Europe indicate that MIS 7d was associated with very dry and cold conditions (Roucoux et al., 2008). MIS 7d is not recorded by significant mass sediment accumulation in the Bay of Biscay suggesting that fluvial discharge through the Fleuve Manche was limited at this time with peaks in the planktic polar foraminifera *N. pachyderma* and Ti/Ca ratios indicating severe cold conditions (Toucanne et al. 2009a; Fig. 5). MIS 7d is associated with a major trough in Northern Hemisphere summer radiation, the lowest of the past 800 ka. The brevity of the stadial is likely to be explained by the subsequent peak in solar radiation in the Northern Hemisphere, which was the highest of the past 800 ka (Fig. 4).

The problem of defining glacial–interglacial cycles using the marine isotope record is further compounded by the recognition or nonrecognition of terminations. Technically, MIS 7d could be classified as part of a glacial–interglacial cycle based on terminations, because it is bounded by terminations III (243 ka) (McManus et al., 1999; Lisiecki and Raymo, 2005) and IIIa (225 ka) (Cheng et al., 2009). The age of IIIa at 225 ka, derived from U-series dating of a Chinese speleothem (Cheng et al., 2009), differs from the marine isotope

https://doi.org/10.1017/qua.2019.76 Published online by Cambridge University Press

curve, which shows a typical sharp transition slightly later at ca. 220–219 ka. This may be an artefact of the age model used in the Lisiecki and Raymo (2005) LR04 stack. In fact, Cheng et al. (2009) found that variations in other marine isotope records, such as that at ODP 980 (McManus et al., 1999), were 3 ka too young when compared with high-resolution dated speleothem records.

MIS 7d represents an anomaly for the preceding and succeeding glacial–interglacial cycles of MIS 9a–8 and MIS 6, because Hughes and Gibbard (2018) defined these cycles as spanning terminations IV–III and IIIa–II, respectively. In this sense, MIS 7d and the interval between terminations III and IIIa represent a truly "missing" glaciation if defined using terminations as the bounding criteria. The main characteristic that defines MIS 7d as a stadial, rather than a full glaciation, is its length, which between terminations III and IIIa is just 18 ka, compared with 76–118 ka for the last 10 "full" glacial–interglacial cycles.

MIS 15b, 13b, and 7d are associated with high or rising eccentricity and the associated pronounced high-amplitude fluctuations in precession (Fig. 4). The intervals began with major solar troughs followed by equally large upswings in solar radiation through ca. 600–580 ka and 240–220 ka in the Northern Hemisphere. At the end of MIS 15b, the Northern Hemisphere summer insolation reached one of the highest peaks of the last million years, similar to at the end of MIS 7d as noted earlier. This pattern of solar radiation changes would have prevented Northern Hemisphere ice expansion achieving the magnitude reached during full glacial–interglacial cycles. In the case of MIS 15, this pronounced insolation peak would also have impacted on the development of the following glacial–interglacial cycles encompassing MIS 14, as noted earlier. This highlights how important Northern Hemisphere insolation is in driving glaciations and the structure of glacial–interglacial cycles. While Hughes and Gibbard (2018) found that changes in Northern Hemisphere insolation account for ca. 50%–60% of global glacial changes, the rest is accounted for in regional internal factors. However, that is for 100 ka glacial–interglacial cycles; for short "missing" glacial intervals like MIS 15b,13b, and 7d, the role of insolation is likely to be even more critical in preventing the development of full glacial–interglacial cycles.

DISCUSSION

"Missing glaciations"—real or apparent?

The hypothesis that global glacial extents were significantly more limited in some glacial–interglacial cycles than others has been tested using a variety of different records. The first and obvious place to look is in the terrestrial record, and here there is notably limited evidence of major global glacial extents in MIS 8, 10, and 14. However, this is not to say that there is no evidence of glaciation in intervals such as MIS 8, only that the patterns of global glaciation do not match those of other glacial–interglacial cycles such as MIS 5d-2, 6, and 12. Indeed, in some areas like northeast Asia and Patagonia, MIS 8 was characterised by a major glacial advance. A key challenge is understanding the true age of the pre-Illinoian glaciations in North America, for which conclusive evidence remains elusive (Rovey and Balco, 2011). Nevertheless, evidence here and in Europe points to MIS 6 being a larger glaciation than both MIS 10 and 8 in most regions.

The terrestrial record of glaciations can potentially provide a misleading impression of the extent of glaciations during different glacial–interglacial cycles, especially where glacial limits were overridden by later glaciers. Even if this was the case, some "missing glaciations" may have been characterised by ice extents that were similar in size to those in later glaciations. However, MIS 8, 10, and 14 were all characterised by much smaller global sea-level depressions, especially MIS 8 and 14 (Table 1), which supports the idea that these were characterised by glaciers that were relatively limited in extent and volume compared with other glacial–interglacial cycles. Dust records also provide insights into the patterns of ice buildup in these glaciations compared with larger glaciations. In the "missing glaciations," dust peaks indicate an early global glacial advance that had more impact on the global hydrological cycle than later in the glacial–interglacial cycle. In the largest glaciations of MIS 5d-2, 6, 12, and 16, the dust peaks were towards the end of glacial–interglacial cycles at the global glacial maxima. The early dust peaks in these big glaciations appear to be associated with glacial advances in high-latitude Asia and globally in the mid-latitude mountains, whereas the later dust peaks correspond with maxima of the large continental ice sheets over North America and Europe (Hughes and Gibbard, 2015; 2018). In the "missing glaciations," it appears that these early glacial advances had bigger impacts on Antarctic dust flux than the later global glacial maxima. Thus, this analogue suggests that during the "missing glaciations" of MIS 8, 10, and 14, the ice sheets of North America and Europe had much less effect on Antarctic dust flux than in the more extensive glaciations of MIS 5d-2, 6, 12, and 16.

While global glacial extents during MIS 8 and 10 are argued to have been less than in other glacial–interglacial cycles, these intervals are associated with a large IRD signal in North Atlantic marine sediment sequences (McManus et al., 1999). This is in contrast to the muted signal of the Fleuve Manche fluvial discharge through the English Channel during these glaciations (Fig. 5). The large IRD signals in MIS 8 and 10 are related to major fluctuations in high-latitude ice sheet margins around the North Atlantic, whereas the Fleuve Manche signal is related to ice sheet margins further south in the mid-latitudes. Some of these margins are associated with the same ice sheets, such as the British–Irish Ice Sheet. The apparent contradiction of high IRD in the northeastern Atlantic (McManus et al., 1999), yet limited fluvial discharge associated with Fleuve Manche (Toucanne et al., 2009a) suggests a different ice configuration than in later glaciations. While North Atlantic IRD at sites farther south and west than ODP 980 is usually dominated by a North American source, background levels of IRD have been linked to the British–Irish Ice Sheet (Bigg et al.,

https://doi.org/10.1017/qua.2019.76 Published online by Cambridge University Press

2010). On the continental margin offshore of Ireland, radiogenic isotope source fingerprinting, in combination with coarse lithic component analysis, indicates a dominant IRD source from the British–Irish ice sheet since the earliest Pleistocene (Thierens et al., 2012). It is therefore possible that the ice sheets over Ireland and Scotland in MIS 8 and 10 were very active, possibly reaching the Atlantic continental shelf, as in the last glacial–interglacial cycle (Stoker and Bradwell, 2005; Bradwell et al., 2007; Peters et al., 2016), but that this was not matched by extensive ice farther east over England and Wales or continental Europe. Thus, the contrasting evidence for glaciation in MIS 8 and 10 from the high- and mid-latitudes in the northeast Atlantic region, as well as across the globe, hints at a major difference in ocean–atmosphere configuration compared with other glacial–interglacial cycles.

The different ocean–atmosphere configurations in MIS 10 and 8 compared with other glaciations in MIS 12, 6, and 5d-2 may be linked to ocean circulation in the North Atlantic and especially North Atlantic deep-water formation. This is known to be affected by the flux of water from the south (Gutjahr et al., 2010), and thus ice sheet–ocean dynamics around Antarctica may have played a significant role in explaining the instability of Northern Hemisphere ice masses in MIS 8 and 10. In fact, as noted earlier, dust flux over Antarctica for MIS 8 was one of the largest and most sustained of the last million years, reaching values comparable with MIS 6 and greater than in MIS 5d-2. This may therefore indicate that global ice volume in MIS 8 was dominated by Southern Hemisphere ice expansion. There is strong evidence of a large glacial advance in Patagonia at ca. 270-260 ka around the time of maximum dust flux over Antarctica (Fig. 4). However, elsewhere, the evidence for MIS 8 is not so clear in Australasia, with glaciations MIS 6 and 10 appearing to be larger. Hein et al. (2017, p. 93) wrote that the "cause of the large MIS 8 advance in central Patagonia during a comparatively minor global ice age is unclear, and is an avenue for future research."

Evidence from the Stocking Glacier in the McMurdo Dry Valleys in eastern Antarctica shows that the glacier was 20%–30% larger than today at 391 ± 35 ka, during MIS 11 (Swanger et al., 2017). It also illustrates that the Dry Valleys have been ice-free for at least the last 350–400 ka. This is important, because it suggests that expansion of the East Antarctic Ice Sheet cannot have been a major factor in explaining differences between the last four 100 ka glacial–interglacial cycles. Instead, it is the smaller and more dynamic West Antarctic Ice Sheet that is most likely to have varied between these glacial–interglacial cycles. West Antarctica is surrounded by the largest area of continental shelf around the continent, with large areas available for ice growth; much larger than around the East Antarctic ice sheet relative to the current size of the respective ice sheets (Amblas and Dowdeswell, 2018) (Fig. 7). The West Antarctic Ice Sheet has long been considered to be prone to collapse (Mercer 1984; Pollard and DeConto 2009). The shelf configuration around this region is equally likely to have facilitated rapid and extensive ice buildup during periods of low global sea

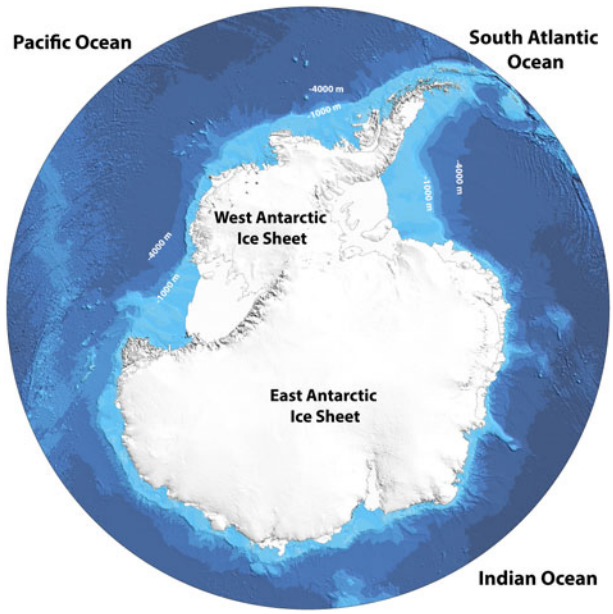

Figure 7. (color online) Topographic map of Antarctica showing offshore bathymetry. The largest area of the currently unglaciated continental shelf is off West Antarctica (Amblas and Dowdeswell, 2018). This means that there was likely to have been greater scope for ice sheet expansion to the shelf edge during Pleistocene glaciations than around the East Antarctic Ice Sheet. Thus, the West Antarctic Ice Sheet would have been the most significant ice mass in the Southern Hemisphere in terms of changing dynamics through glacial–interglacial cycles. From the International Bathymetric Chart of the Southern Ocean (IBCSO), version 1.0, www.scar.org/science/ibcso/resources (Arndt et al., 2013).

levels during glaciations. It has been suggested that the West Antarctic Ice Sheet shifted to a marine-based configuration after the Early–Middle Pleistocene transition (Sutter et al., 2019), and it is likely that the nature of this configuration through different subsequent glacial–interglacial cycles would have been a major factor in influencing ice sheet dynamics. However, most glacial geologic studies of the West Antarctic Ice Sheet relate to the last glacial–interglacial cycle (e.g., Sugden et al., 2006) with little direct evidence of Middle Pleistocene glacial histories.

Given this evidence, any Southern Hemisphere lead associated with Antarctica must be associated with changes in the West Antarctic Ice Sheet. This is in terms of both ice sheet–atmosphere and ice sheet–ocean interactions, the latter influencing climate in the Northern Hemisphere through both the thermal ocean seesaw (Crowley 1992; Stocker and Johnsen, 2003; Pedro et al., 2018) and the deep-water seesaw (Broecker, 1998). Increased freshwater input from ice sheets as they expanded to the continental shelf, causing greater calving loss, is likely to have had a major impact on the Antarctic meridional overturning current, which in turn affects the strength of North Atlantic deep-water formation (Swingedouw et al., 2009).

Thus, extensive West Antarctic Ice Sheets in MIS 8 and 10 may have reduced the strength of the North Atlantic

https://doi.org/10.1017/qua.2019.76 Published online by Cambridge University Press

conveyor, inhibiting moisture delivery to the areas of potential ice sheet growth in lands bordering the North Atlantic Ocean. In this scenario, the early dust peak maxima in both MIS 10 and 8 (Fig. 4) would be caused by the Southern Hemisphere lead in ice buildup, which was matched by ice buildup in the Northern Hemisphere, especially over Asia. However, as West Antarctic ice grew larger through the glacial–interglacial cycle, this caused a shutdown of the North Atlantic conveyor, starving ice sheets around the North Atlantic Ocean of moisture, thus explaining their absence from the geologic record. This pattern is best suited to explain the nature of glaciations in MIS 8, because the early dust peak is also matched by the lowest global sea levels, which both precede the benthic $\delta^{18}O$ trough by ca. 18 ka. While MIS 10 exhibited some similarities to MIS 8, it also had similarities with the larger glacial extents of MIS 12, 6, and 5d-2. MIS 14, on the other hand, has strong similarities with MIS 8, especially because both are followed by extended interglacial complexes (MIS 13 and 7, respectively). Hao et al. (2015) argued that MIS 14 inception was a response to changes in Antarctic ice sheets rather than to Northern Hemisphere cooling. However, in MIS 14 it is likely that the West Antarctic Ice Sheet was more restricted and sensitive than in MIS 10 and 8, as there is evidence that the ice sheet collapsed in the MIS 15–13 interval (Hillenbrand et al., 2009). This is possibly due to significantly higher global sea levels during MIS 14 than occurred in other major glaciations (Table 1).

The relatively weak signal of global glaciation within MIS 14 has also been proposed as a direct cause of the extended interglacial complex of MIS 15–13 (Hao et al., 2015). While the strong solar radiation peak that preceded this glaciation in MIS 15a would have mitigated glacial inception in MIS 14, the subsequent weak global glaciation would also have an impact on the extended interglacial that followed (MIS 13). This is also evident in the case of MIS 8, a weak global glaciation that was followed by the extended interglacial complex of MIS 7. This observation also has relevance for subsequent glacial inception, with some cases of failed glacial–interglacial cycles evident in intervals such as MIS 13b and 7d, which succeeded the weak glaciations in MIS 14 and 8, respectively.

Looking for patterns: the role of orbital forcing in explaining the magnitude of glaciations

There is a clear link between the magnitude of peak–trough variations at the end of interglacials and the intensity of global glaciations in the subsequent cold stage. This is evident in the values of solar-trough magnitude for the last seven glacial–interglacial cycles (Table 2). MIS 8 and 10 are associated with the lowest values of solar-trough magnitude. Lower solar-trough magnitudes at the end of interglacials mean that glacial buildup early in the glacial cycles is likely to be less significant than in other glacial–interglacial cycles in which solar-trough magnitudes are more pronounced (Table 2). MIS 14 does not conform with this hypothesis, because it was characterised by a large solar-trough magnitude at the end of MIS 15. However, the preceding solar radiation peak was the largest preceding any of the last seven glacial–interglacial cycles and was associated with maximum eccentricity (Fig. 4). In fact, in the last 800 ka, solar radiation only exceeded the MIS 15 peak in the Northern Hemisphere summer in the extended interglacial complex of MIS 7 (Fig. 4).

As noted earlier, the drivers of global glacial dynamics during the weaker global glaciations in MIS 8 and 14 appear to have had a southern lead and to have been dominated by changes in Antarctic ice sheets rather than by Northern Hemisphere cooling. This suggests that a Northern Hemisphere lead in driving global glaciations through solar forcing is mitigated by interhemispheric ocean–atmosphere connections. This partly explains why changes in Northern Hemisphere solar radiation can only explain 50%–60% of global ice volume through the last 100 ka glacial–interglacial cycles (see Hughes and Gibbard, 2018). The evidence also suggests that changes in Northern Hemisphere solar radiation have a much smaller influence in explaining glacial dynamics during the "missing glaciations," such as MIS 8 and 14. While there was a northern lead and quasi-synchronicity in climate for the most severe and largest glaciations of MIS 16, 12, 6, and 5d-2, driven by changes in solar radiation input to the Northern Hemisphere (e.g., Mercer, 1984), this was not the case for the "missing glaciations" of MIS 14, 10, and 8. This is important, because it shows that solar forcing was not a significant control on global glaciation during the "missing glaciations." It illustrates that the Milankovitch hypothesis cannot explain the structure of all glacial cycles—a point noticed several decades ago (see references in Mercer, 1984). This is still a significant issue today, because the marine isotope record is still tuned to the pacing of orbital variations (Lisiecki and Raymo, 2005) following the findings of Hays et al. (1976). While this is appropriate for the classic 100 ka glacial cycles such as MIS 16, 12, 6, and 5d-2, the efficacy of orbital tuning breaks down when dealing with "missing glaciations" such as MIS 14, 10, and 8. This, and the fact that the marine oxygen isotope record suffers from spatial bias (i.e., the dominance of the Laurentide Ice Sheet), means that the established view of glacial–interglacial cycles through the lens of the marine isotope curve can be misleading.

There is a potential link between orbital eccentricity and the magnitude of glaciations over the last six glacial–interglacial cycles. Increasing eccentricity causes increasing amplitude of variations in the climatological precession parameter ($e \sin \omega$) that describes how the precession of the equinoxes affects the seasonal configuration of the Earth–Sun distance (Berger and Loutre, 1991, p. 297). This affects the solar-trough magnitude at the end of interglacials (Fig. 4). Small glaciers can rapidly build up in response to mass-balance changes associated with a deteriorating climate (Bahr et al., 1998). This explains why mountain glaciers are often seen to reach their maxima early in glacial–interglacial cycles when precession contrasts were at their greatest (see Hughes et al., 2013; Hughes and Gibbard, 2018). However,

https://doi.org/10.1017/qua.2019.76 Published online by Cambridge University Press

precessional cycles are too short to sustain larger ice sheet buildup. This means that ice sheets are more likely to sustain buildup during periods of low precessional variability. This was the case in MIS 12, for example (Fig. 4). Another important consideration is the effect of diminishing magnitude of precessional cycles through glacial–interglacial cycles, which is displayed during some of the largest glaciations, such as in MIS 12 and 5d-2 (Fig. 4). In contrast, this effect is much weaker or reversed (i.e., increasing magnitude of precessional cycles) during MIS 8 and 10, respectively. Diminishing precession, as seen in MIS 12 and 5d-2, results in excess ice buildup, causing ice sheet instability and collapse during terminations after the fourth or fifth precessional cycles (Raymo, 1997; Ridgwell et al., 1999). This is because diminished precession causes smaller changes between the seasons, and the negative effects on glacial mass balance of the lengthening of the melt season during upswings to solar peaks is reduced (Hughes and Gibbard, 2018).

The sets of consecutive "missing glaciations" in MIS 10 and 8 occurred during a trend towards increasing eccentricity and precession that caused larger amplitude variations in solar radiation, which reached their greatest amplitude in MIS 7 (Fig. 4). Other "missing glaciations" in the weak pseudo glacial–interglacial cycles of MIS 7d, 13b, and 15b also correspond with large-amplitude solar cycles associated with increased eccentricity and associated precession. This pattern supports the idea that glaciations are influenced by 413 ka cycles with 100 ka glacial–interglacial cycles superimposed and modulated by these larger-scale orbital cycles (Rial, 1999). However, the relationship is not perfect, because MIS 16, one of the major global glaciations, also occurred during a rising trend of eccentricity (Fig. 4), although this earlier eccentricity cycle was less pronounced than that which occurred over the last six glacial–interglacial cycles, and the effects on precession were smaller.

"Missing glaciations" and implications for Quaternary chronostratigraphy

The fact that not all 100 ka glacial–interglacial cycles produced the same magnitude of ice extent and volume on Earth has major implications for understanding how these cycles relate to glaciations. This is complicated further when considering shorter-term climatic variations and their global glacial imprint. For example, despite being classified within isotope interglacials, MIS 7d, 13b and 15b saw global sea-level depressions similar to some glacial maxima within full glacial–interglacial cycles, such as MIS 14 for example. This highlights the problems of using single proxy records, largely dominated by the marine isotope record, as a measure of the extent and pacing of global glaciations. The fact that marine isotope sequences are tuned by orbital parameters provides a sense of regularity around glacial–interglacial cycles when it is apparent that not all glacial–interglacial cycles are the same, with some very different from others. The lesson from this is that the extent and magnitude of glaciations within glacial–interglacial cycles cannot be deciphered using the marine isotope record alone. This further highlights the problems of correlating terrestrial sequences with the marine isotope record (see Gibbard and West, 2000) and is a problem not limited to just glacial records (e.g., Biñka and Marks, 2018).

For example, for one of the most extensive glaciations of the Quaternary, the Saalian, Wolstonian, Illinoian, and equivalents (during MIS 6), both the timing and extent of individual regional glacial advances and retreats vary significantly. In northern Europe, two major stadial advances are recognised during the classical Saalian glaciation, the Late Saalian Drenthe and Warthe Stadial advances, lasting from ~175–155 and 150–135 ka, respectively (Toucanne et al., 2009a; Margari et al., 2014) (Fig. 6). In the past, these events had been thought to represent separate glaciations; however, there is no evidence of major interglacial warming during the intervening interval (Ehlers et al., 2011c). While robust dating now indicates that the two major intervals occurred during the same glaciation, marine records indicate that after ~150 ka, ice sheets expanded, with global ice volume reaching the penultimate glacial maximum extent towards the end of MIS 6 (i.e., ~140 ka). This principally reflects the growth of the late Illinoian ice sheet in North America (e.g., Curry et al., 2011; Syverson and Colgan, 2011; Margari et al., 2014). However, in Europe the equivalent Warthe ice advance was markedly less extensive than the Drenthe/Dniepr, although this might have been compensated for by glacial expansion in Russia and Siberia (e.g., Astakhov, 2004). Likewise, the apparent absence of glaciation during MIS 8 (Middle Saalian/pre-Illinoian A) in both western Europe and North America contrasts with the record in the east, such as in Siberia, where the ice reached its Pleistocene maximum extent at that time.

In recent publications on the Quaternary stratigraphy of northern Germany, and to some extent elsewhere, references to the correlation with marine isotope stages are largely avoided. The number of interglacials between the Elsterian and Saalian is still disputed, but the position of the Holsteinian Stage interglacial has gradually moved from MIS 7 (Caspers et al., 1995), via MIS 9 (Litt et al., 2007), to MIS 11 (Ehlers, 2011; Stephan, 2014). If the latter interpretation is correct, except for the Treldenæs Till in Jutland (Denmark), no truly glacial deposits of either MIS 10 or 8 have been identified so far. In the British Isles, the equivalent of the Saalian Stage interval is defined as the Wolstonian in a borehole at Marks Tey in East Anglia. As in Germany (cf. Stephan, 2014), the Wolstonian Stage has been plagued by incorrect correlations with the marine isotope record because of the climatic complexity within it. This is despite Gibbard and Turner (1990) stating that "the Wolstonian Stage includes all time between the end of the Hoxnian [~MIS 11] and the beginning of the Ipswichian [~MIS 5] Stages irrespective of climatic or similar events that may be subsequently identified." The evidence presented here shows that while there is no doubt that multiple such climatic and glaciation events occurred in MIS 10 and 8, their imprint in the terrestrial sequences is

https://doi.org/10.1017/qua.2019.76 Published online by Cambridge University Press

frequently lacking, and this highlights why glaciations are time-transgressive events and should not be confused with true chronostratigraphic units in the Quaternary stratigraphic record.

Another consequence of the observations presented here is that for older glaciations, in common with those of the last glacial–interglacial cycle (Weichselian, Wisconsinan, Valdaian, etc.; Hughes et al., 2013; Hughes and Gibbard, 2018), it cannot be assumed that ice sheets throughout the world reached their maximum extents at the same time. Rather it appears that asynchroneity is the norm, at least during the major glaciations of the Middle to Late Pleistocene. All these results clearly emphasise the danger of adopting a simplistic counting backward-and-forward approach to extraregional glacial stratigraphy. Indeed, the implications for stratigraphic and modelling reconstructions are profound. The lesson being that simple, one-to-one, uncritical correlations with terrestrial, and in particular with the marine isotope sequences, hold many potentially serious pitfalls for the unwary.

CONCLUSIONS

Glaciations in MIS 8 and 10 were relatively limited in extent in western Europe and North America in comparison to other Middle Pleistocene glaciations such as the Elsterian/pre-Illinoian B (MIS 12) and the Late Saalian/Illinoian (MIS 6). MIS 14 was especially marginal as a glacial–interglacial cycle compared with other 100 ka cycles in terms of glacial extent and related global climatic and environmental indicators. In most areas, glaciations were less extensive in MIS 8, 10, and 14 than the Weichselian/Wisconsinan (MIS 5d-2), with a few notable exceptions. For example, east of the Urals in Siberia, the maximum extent of MIS 8 glaciation marks the maximum extent of Pleistocene glaciation in this region. Also, in parts of Patagonia, MIS 8 glaciers were larger than in both MIS 6 and 5d-2.

The records for MIS 8 and 10 differ from other glacial–interglacial cycles in that there is evidence of pronounced dust peaks in Antarctic ice cores early on, with smaller dust peaks towards the end of the glacial–interglacial cycles during global glacial maxima. The early dust peak in the last glacial–interglacial cycle (MIS 5d-2) is associated with early advances of glaciers in the mid-latitude mountains, continental interiors, and especially Arctic Asia and mountains bordering the northwest Pacific Ocean (Hughes et al., 2013; Batchelor et al., 2019). By analogy, this implies that MIS 8 and 10 saw large glaciations in these regions but less significant continental ice sheet expansions around the North Atlantic margins. This is supported by sea-level evidence, with global sea-level depressions ca. 20–40 m less in MIS 8 and 10 compared with those during MIS 12, 6, and 2. However, early dust peaks in MIS 8 are also closely related to significant ice expansion in Patagonia, suggesting a Southern Hemisphere lead. The relationship between Southern and Northern Hemisphere glaciations is likely to be affected by the dynamics of the West Antarctic Ice Sheet and the effects of its expansion on ocean circulation through oceanic bipolar seesaws.

Solar forcing plays a major role in determining the size and length of glaciations. Over the long term, the "missing glaciations" of the last six glacial–interglacial cycles are associated with rising eccentricity and increased precession. While this accelerates glacial buildup in the short term during pronounced insolation downturns, it hinders buildup during the following upswing. For example, the amplitude of solar precession associated with peak eccentricity can be linked to failed glacial–interglacial cycles such as MIS 7d and 15b. These short intense stadials were prevented from developing into full glacial–interglacial cycles directly because of the pattern of Northern Hemisphere solar variations.

The fact that 100 ka glacial–interglacial cycles produced glaciations of very different magnitudes in different places around the globe poses problems when relying on a global indicator of glacial change, as is often the case when using the marine isotope record. This has important implications for using the marine isotope record as a basis for understanding glaciations on land and wider terrestrial records. The structure of glacial–interglacial cycles, while predictable when considering the largest glaciations, is much less clear when considering weaker global glaciations in MIS 8, 10, and 14. The spatial and temporal patterns of glaciation were different in these glacial–interglacial cycles compared with the strongest glaciations of the last 500 ka in MIS 12, 6, and 5d-2. This indicates that glacial–interglacial cycles are not as predictable as is suggested in marine isotope records that are tuned by orbital cycles.

ACKNOWLEDGMENTS

We thank Senior Editor Nicholas Lancaster, Associate Editor Pat Bartlein, and two anonymous reviewers for detailed and very helpful comments on an initial draft of this paper. We also thank Graham Bowden and Nick Scarle for drawing the figures.

REFERENCES

Amblas, D., Dowdeswell, J.A., 2018. Physiographic influences on dense shelf-water cascading down the Antarctic continental slope. *Earth Science Reviews* 185, 887–900.

Arndt, J.E., Schenke, H.W., Jakobsson, M., Nitsche, F., Buys, G., Goleby, B., Rebesco, M., *et al*., 2013. The International Bathymetric Chart of the Southern Ocean (IBCSO) Version 1.0—a new bathymetric compilation covering circum-Antarctic waters. *Geophysical Research Letters* 40, 3111–3117.

Astakhov, V., 2004. Pleistocene ice limits in Russian northern lowlands. In: Ehlers, J., Gibbard, P.L. (Eds.), *Quaternary Glaciations—Extent and Chronology*. Part 1, *Europe*. Developments in Quaternary Sciences 2. Elsevier, Amsterdam, pp. 309–319.

Astakhov, V., 2011. Ice margins of northern Russia revisited. In: Ehlers, J., Gibbard, P.L., Hughes, P.D. (Eds.), *Quaternary Glaciations—Extent and Chronology: A Closer Look*. Developments in Quaternary Sciences 15. Elsevier, Amsterdam, pp. 1–14.

Astakhov, V., Shkatova, V., Zastrozhnov, A., Chuyko, M., 2016. Glaciomorphological map of the Russian Federation. *Quaternary International* 420, 4–14.

https://doi.org/10.1017/qua.2019.76 Published online by Cambridge University Press

Bahr, D.B., Pfeffer, W.T., Sassolas, C., Meier, M.F., 1998. Response time of glaciers as a function of size and mass balance: 1. *Theory.* Journal of Geophysical Research 103, 9777–9782.

Barendregt, R.W., Duk-Rodkin, A., 2011. Chronology and extent of late Cenozoic ice sheets in North America: a magnetostratigraphical assessment. In: Ehlers, J., Gibbard, P.L., Hughes, P.D. (Eds.), *Quaternary Glaciations—Extent and Chronology, A Closer Look*. Developments in Quaternary Sciences 15. Elsevier, Amsterdam, pp. 419–426.

Barrell, D.J.A., 2011. Quaternary glaciers of New Zealand. In: Ehlers, J., Gibbard, P.L., Hughes, P.D. (Eds.), *Quaternary Glaciations—Extent and Chronology: A Closer Look*. Developments in Quaternary Sciences 15. Elsevier, Amsterdam, pp. 1047–1064.

Barrows, T.T., Stone, J.O., Fifield, L.K., Cresswell, R.G., 2002. The timing of the last glacial maximum in Australia. *Quaternary Science Reviews* 21, 159–173.

Batchelor, C.L., Margold, M., Krapp, M., Murton, D.K., Dalton, A.S., Gibbard, P.L., Stokes, C.R., Murton, J.B., Manica, A., 2019. The configuration of Northern Hemisphere ice sheets through the Quaternary. *Nature Communications* 10:3713.

Beets, D., Meijer, T., Beets, C., Cleveringa, P., Laban, C., van der Spek, A., 2005. Evidence for a middle Pleistocene glaciation of MIS 8 age in the southern North Sea. *Quaternary International* 133–134, 7–19.

Berger, A., 1992. *Orbital Variations and Insolation Database*. IGBP PAGES/World Data Center for Paleoclimatology Data Contribution Series # 92-007. NOAA/NGDC Paleoclimatology Program, Boulder, CO.

Berger, A., Loutre, M.F., 1991. Insolation values for the climate of the last 10 million years. *Quaternary Sciences Reviews* 10, 297–317.

Bigg, G.R., Levine, R.C., Clark, C.D., Greenwood, S.L., Haflidason, H., Hughes, A.L.C., Nygård, A., Sejrup, H.P., 2010. Last glacial ice-rafted debris off southwestern Europe: the role of the British–Irish Ice Sheet. *Journal of Quaternary Science* 25, 689–699.

Biñka, K., Marks, L., 2018. Terrestrial versus marine archives: biostratigraphical correlation of the Middle Pleistocene lacustrine records from central Europe and their equivalents in the deep-sea cores from the Portuguese margin. *Geological Quarterly* 62, 69–80.

Bintanja, R., Roderik, S.W., van de Wal, O.J., 2005. Modeled atmospheric temperatures and global sea levels over the past million years. *Nature* 437, 125–128.

Bolliger, T., Feijfar, O., Graf, H.R., Kalin, D.W., 1996. Vorläufige Mitteilung über Funde von pliozanen Kleinsäugern aus den Höheren Deckenschottern des Irchels (Kt. Zürich). *Eclogae geologicae Helvetiae* 89, 1043–1048.

Bolshiyanov, D.Y., Savatuygin, L.M., Shneider, G.V., Molodkov, A.N., 1998. New data about modern and ancient glaciations of the Taimyro-Severozemlskaya region. [In Russian.] *Materialny glyatchiologicheskich issledovanii* 85, 219–222.

Bradwell, T., Stoker, M., Larter, R., 2007. Geomorphological signature and flow dynamics of the Minch palaeo-ice stream, NW Scotland. *Journal of Quaternary Science* 22, 609–617.

Braun, D., 2011. The glaciation of Pennsylvania, USA. In: Ehlers, J., Gibbard, P.L., Hughes, P.D. (Eds.), *Quaternary Glaciations—Extent and Chronology: A Closer Look*. Developments in Quaternary Sciences 15. Elsevier, Amsterdam, pp. 521–530.

Bridgland, D.R., Howard, A.J., White, M.J., White, T.S. (Eds.), 2014. *Quaternary of the Trent*. Oxbow Books, Oxford.

Broecker, W.S., 1998. Paleocean circulation during the last deglaciation: a bipolar seesaw? *Paleoceanography* 13, 119–121.

Broecker, W.S., van Donk, J., 1970. Insolation changes, ice volumes, and the O^{18} record in deep-sea cores. *Reviews of Geophysics* 8, 169–198.

Calvet, M., 2004. The Quaternary glaciations of the Pyrenees. In: Ehlers, J., Gibbard, P. L. (Eds.): *Quaternary Glaciations—Extent and Chronology.* Part 1, *Europe.* Developments in Quaternary Sciences 2. Amsterdam, Elsevier, pp. 119–128.

Caspers, G., Jordan, H., Merkt, J., Meyer, K.-D., Müller, H., Streif, H., 1995. Niedersachsen. In: Benda, L. (Ed.), *Das Quartär Deutschlands*. Borntraeger, Stuttgart, pp. 23–58.

Cheng, H., Edwards, L., Broecker, W.S., Denton, G.H., Kong, X., Wang, Y., Zhang, R., Wang, X., 2009. Ice age terminations. *Science* 326, 248–252.

Claquin, T., Roelandt, C., Kohfeld, K., Harrison, S., Tegen, I., Prentice, I., Balkanski, Y., *et al*., 2003. Radiative forcing of climate by ice-age atmospheric dust. *Climate Dynamics* 20, 193–202.

Clark, P.U., Pollard, D., 1998. Origin of the Middle Pleistocene transition by ice sheet erosion of regolith. *Paleoceanography* 13, 1–9.

Cohen, K.M., Gibbard, P., 2011. *Global Chronostratigraphical Correlation Table for the Last 2.7 Million Years*. Subcommission on Quaternary Stratigraphy (International Commission on Stratigraphy), Cambridge, UK. http://quaternary.stratigraphy.org/charts.

Colhoun, E.A., 1985. The glaciations of the West Coast Range, Tasmania. *Quaternary Research* 24, 39–59.

Colhoun, E.A., Barrows, T.T., 2011. The glaciation of Australia. In: Ehlers, J., Gibbard, P.L., Hughes, P.D. (Eds.), *Quaternary Glaciations—Extent and Chronology: A Closer Look*. Developments in Quaternary Sciences 15. Elsevier, Amsterdam, pp. 1037–1045.

Crowley, T., 1992. North Atlantic deepwater cools the Southern Hemisphere. *Paleoceanography* 7, 489–497.

Curry, B.B., Grimley, D.A. and McKay, E.D., III, 2011, Quaternary glaciations in Illinois. In: Ehlers, J., Gibbard, P.L., Hughes, P.D. (Eds.), *Quaternary Glaciations—Extent and Chronology: A Closer Look*: Developments in Quaternary Sciences 15. Elsevier, Amsterdam, pp. 467–487.

Davies, B.J., Roberts, D.H., Bridgland, D.R., Ó Cofaigh, C., Riding, J.B., Demarchi, B., Penkman, K., Pawley, S.M., 2012. Timing and depositional environments of a Middle Pleistocene glaciation of northeast England: new evidence from Warren House Gill, County Durham. *Quaternary Science Reviews* 44, 180–212.

Demuro, M., Froese, D., Arnold, L., Roberts, R., 2012. Single-grain OSL dating of glaciofluvial quartz constrains Reid glaciation in NW Canada to MIS 6. *Quaternary Research* 77, 305–316.

Doppler, G., Kroemer, E., Rögner, K., Wallner, J., Jerz, H., Grottenthaler, W., 2011. Quaternary stratigraphy of southern Bavaria. *E&G Quaternary Science Journal* 60(2–3), 329–365.

Duk-Rodkin, A., Barendregt, R.W., 2011. Stratigraphical record of glacials/interglacials in Northwest Canada. In: Ehlers, J., Gibbard, P.L., Hughes, P.D. (Eds.), *Quaternary Glaciations—Extent and Chronology: A Closer Look*. Developments in Quaternary Sciences 15. Elsevier, Amsterdam, pp. 661–698.

Duk-Rodkin, A., Barendregt, R.W., Froese, D.G., Weber, F., Enkin, R.J., Smith, I.R., Zazula, G.D., Waters, P., Kalssen, R., 2004. Timing and extent of Plio-Pleistocene glaciations in North-Western Canada and East-Central Alaska. In: Ehlers, J., Gibbard, P.L. (Eds.), *Quaternary Glaciations—Extent and*

https://doi.org/10.1017/qua.2019.76 Published online by Cambridge University Press

Chronology. Part 2, *North America*. Elsevier, Amsterdam, pp. 313–345.

Dyke, A.S., Prest, V.K., 1987. Late Wisconsinan and Holocene history of the Laurentide Ice Sheet. *Géographie Physique et Quaternaire* 41, 237–263.

Ehlers, J., 2011. *Das Eiszeitalter*. Spektrum, Heidelberg.

Ehlers, J., Gibbard, P.L., 2007. The extent and chronology of Cenozoic Global Glaciation. *Quaternary International* 164–165, 6–20.

Ehlers, J., Gibbard, P.L., Hughes, P.D. (Eds.), 2011a. *Quaternary Glaciations—Extent and Chronology: A Closer Look*. Developments in Quaternary Sciences 15. Elsevier, Amsterdam. 1108 pp.

Ehlers, J., Gibbard, P.L., Hughes, P.D. (Eds.), 2011b. Introduction. In: Ehlers, J., Gibbard, P.L., Hughes, P.D. (Eds.), *Quaternary Glaciations—Extent and Chronology: A Closer Look*. Developments in Quaternary Sciences 15. Amsterdam: Elsevier. pp. 1–14.

Ehlers, J., Gibbard, P.L., Hughes, P.D., 2018. Quaternary glaciations and chronology. In: Menzies, J., van der Meer, J.J.M. (Eds.), *Past Glacial Environments*. 2nd ed. Amsterdam, Elsevier, pp. 77–101.

Ehlers, J., Grube, A., S. H-J., Wansa, S., 2011c. Pleistocene glaciations of North Germany—new results. In: Ehlers, J., Gibbard, P.L., Hughes, P.D. (Eds.), *Quaternary Glaciations—Extent and Chronology: A Closer Look*. Developments in Quaternary Sciences 15. Amsterdam, Elsevier, pp. 149–162.

Elderfield, H., Ferretti, P., Greaves, M., Crowhurst, S., McCave, N., Hodell, D., Piotrowski, A.M., 2012. Evolution of ocean temperature and ice volume through the mid-Pleistocene climate transition. *Science* 337, 704–709.

Evans, D.J.A., Roberts, D.H., Bateman, M.D., Ely, J., Medialdea, A., Burke, M.J., Chiverrell, R.C., Clark, C.D., Fabel, D., 2019. A chronology for North Sea Lobe advance and recession on the Lincolnshire and Norfolk coasts during MIS 2 and 6. *Proceedings of the Geologists' Association* 130, 523–540.

Fernández Mosquera, D., Marti, K., Vidal Romaní, J.R., Weigel, D., 2000. Late Pleistocene deglaciation chronology in the NW of the Iberian Peninsula using cosmic-ray produced ^{21}Ne in quartz. *Nuclear Instruments and Methods in Physical Research B* 172, 832–837.

Fiebig, M., Ellwanger, D., Doppler, G., 2011. Pleistocene glaciations of southern Germany. In: Ehlers, J., Gibbard, P.L., Hughes, P.D. (Eds.), *Quaternary Glaciations—Extent and Chronology: A Closer Look*. Developments in Quaternary Sciences 15. Elsevier, Amsterdam, pp. 163–174.

Fletcher, W.J., Müller, U.C., Koutsodendris, A., Christanis, K., Pross, J., 2013. A centennial-scale record of vegetation and climate variability from 312 to 240ka (Marine Isotope Stages 9c-a, 8 and 7e) from Tenaghi Philippon, NE Greece. *Quaternary Science Reviews* 78, 108–125.

Fullerton, D.S., Colton, R.B., Bush, C.A., 2004. Limits of mountain and continental glaciations east of the Continental Divide in northern Montana and north-western North Dakota, U.S.A. In: Ehlers, J., Gibbard, P.L. (Eds.), *Quaternary Glaciations—Extent and Chronology*. Part 2, North America. Elsevier, Amsterdam, pp. 131–150.

Ganopolski, A., Calov, R., 2011. The role of orbital forcing, carbon dioxide and regolith in 100 kyr glacial cycles. *Climate of the Past* 7, 1415–1425.

Ganopolski, A., Winkelmann, R., Schellnhuber, H.J., 2016. Critical insolation–CO_2 relation for diagnosing past and future glacial inception. *Nature* 529, 200–203.Gibbard, P.L., Clark, C.D., 2011. Pleistocene glaciation limits in Great Britain. In: Ehlers, J., Gibbard, P.L., Hughes, P.D. (Eds.), *Quaternary Glaciations—Extent and Chronology: A Closer Look*. Developments in Quaternary Sciences 15. Elsevier, Amsterdam, pp. 75–94.

Gibbard, P.L., Turner, C., 1990. Cold stage type sections: some thoughts on a difficult problem. *Quaternaire* 1, 33–40.

Gibbard, P.L., West, R.G., 2000. Quaternary chronostratigraphy: the nomenclature of terrestrial sequences. *Boreas* 29, 329–336.

Gibbard, P.L., West, R.G., Hughes, P.D., 2018. Pleistocene glaciation of Fenland, England, and its implications for evolution of the region. *Royal Society Open Science* 4, 170736.

Gillespie, A., Molnar, P., 1995. Asynchronous maximum advances of mountain and continental glaciers. *Reviews of Geophysics* 33, 311–364.

Gillespie, A.R., Clark, D.H., 2011. Glaciations of the Sierra Nevada, California, USA. In: Ehlers, J., Gibbard, P.L., Hughes, P.D. (Eds.) *Quaternary Glaciations—Extent and Chronology: A Closer Look*. Elsevier, Amsterdam, pp. 447–462.

Gillespie, A.R., Zehfuss, P.H., 2004. Glaciations of the Sierra Nevada, California, USA. In: Ehlers, J., Gibbard, P.L. (Eds.), *Quaternary Glaciations—Extent and Chronology*. Part 2, *North America*. Elsevier, Amsterdam, pp. 131–150.

Giraudi, C., Bodrato, G., Ricci Lucchi, M., Cipriani, N., Villa, I.M., Giaccio, B., Zuppi, G.M., 2011. The Middle and late Pleistocene glaciations in the Campo Felice basin (Central Apennines, Italy). *Quaternary Research* 75, 219–230.

Giraudi, C., Giaccio, B., 2017. Middle Pleistocene glaciations in the Apennines, Italy: new chronological data and preservation of the glacial record. *Geological Society of London Special Publication* 433, 161–178.

Graham, A.G.C., 2007. *Reconstructing Pleistocene Glacial Environments in the Central North Sea Using 3D Seismic and Borehole Data*. PhD thesis, University of London.

Graham, A.G.C., Stoker, M.S., Lonergan, L., Bradwell, T., Stewart, M.A., 2011. The Pleistocene glaciations of the North Sea Basin. In: Ehlers, J., Gibbard, P.L., Hughes, P.D. (Eds.), *Quaternary Glaciations—Extent and Chronology: A Closer Look*. Developments in Quaternary Sciences 15, Elsevier, Amsterdam, pp. 261–278.

Gutjahr, M., Hoogakker, B.A.A., Frank, M., McCave, N., 2010. Changes in North Atlantic deep water strength and bottom water masses during Marine Isotope Stage 3 (45–35 ka BP). *Quaternary Science Reviews* 29, 2451–2461.

Hao, Q., Wang, L., Oldfield, F., Guo, Z., 2015. Extra-long interglacial during MIS 15-13 arising from limited extent of Arctic ice sheets in glacial MIS 14. *Scientific Reports* 5, 12103.

Hays, J.D., Imbrie, J., Shackleton, N.J., 1976. Variations in the Earth's orbit: pacemaker of the ice ages. *Science* 194, 1121–1132.

Head, M.J., Gibbard, P.L., 2005. Early–Middle Pleistocene transitions: an overview and recommendations for the defining boundary. *Geological Society of London Special Publication* 247, 1–18.

Head, M.J., Gibbard, P.L., 2015. Formal subdivision of the Quaternary System/Period: past, present, and future. *Quaternary International* 383, 4–35.

Head, M.J., Pillans, B., Farquhar, S.R., 2008. The Early–Middle Pleistocene transition: characterization and proposed guide for the defining boundary. *Episodes* 31, 255–259.

Hein, A.S., Cogez, A., Darvill, C.M., Mendelova, M., Kaplan, M.R., Herman, F., Dunai, T.J., *et al.*, 2017. Regional mid-Pleistocene glaciation in central Patagonia. *Quaternary Science Reviews* 164, 77–94.

https://doi.org/10.1017/qua.2019.76 Published online by Cambridge University Press

Hein, A.S., Hulton, N.R.J., Dunai, T.J., Schnabel, C., Kaplan, M.R., Naylor, M., Xu, S., 2009. Middle Pleistocene glaciation in Patagonia dated by cosmogenic-nuclide measurements on outwash gravels. *Earth and Planetary Science Letters* 286, 184–197.

Hillenbrand, C.-D., Kuhn, G., Frederichs, T., 2009. Record of a Mid-Pleistocene depositional anomaly in West Antarctic continental sediments: an indicator for ice-sheet collapse. *Quaternary Science Reviews* 28, 1147–1159.

Hobbs, W.W., 1945. The Greenland glacial anticyclone. *Journal of Meteorology* 2, 143–153.

Houmark-Nielsen, M., 2004.The Pleistocene of Denmark: a review of stratigraphy and glaciation history. In: Ehlers, J., Gibbard, P.L. (Eds.), *Quaternary Glaciations—Extent and Chronology*. Part 1, *Europe*. Elsevier, Amsterdam, pp. 35–46.

Houmark-Nielsen, M., 2011. Pleistocene glaciations in Denmark: a closer look at chronology, ice dynamics and landforms. In: Ehlers, J., Gibbard, P.L., Hughes, P.D. (Eds.), *Quaternary Glaciations—Extent and Chronology: A Closer Look*. Developments in Quaternary Sciences 15. Elsevier, Amsterdam, pp. 47–58.

Hughes, P.D., Gibbard, P.L. 2015. A stratigraphical basis for the Last Glacial Maximum (LGM). *Quaternary International* 383, 174–185.

Hughes, P.D., Gibbard, P.L., 2018. Global glacier dynamics during 100 ka Pleistocene glacial cycles. *Quaternary Research* 90, 222–243.

Hughes, P.D., Gibbard, P.L., Ehlers, J., 2013. Timing of glaciation during the last glacial cycle: evaluating the meaning and significance of the "Last Glacial Maximum" (LGM). *Earth Science Reviews* 125, 171–198.

Hughes, P.D., Woodward, J.C., van Calsteren, P.C., Thomas, L.E., 2011. The glacial history of the Dinaric Alps, Montenegro. *Quaternary Science Reviews* 30, 3393–3412.

Imbrie, J., Hays, J.D., Martinson, D.G., McIntyre, A., Mix, A.C., Morley, J.J., Pisias, N.G., Prell, W.L., Shackleton, N.J., 1984. The orbital theory of Pleistocene climate: support from a revised chronology of the marine ^{18}O record. In: Berger, A., Imbrie, J., Hays, G., Kukla, G., Saltzman, B. (Eds.), *Milankovitch and Climate*. Reidel, Dordrecht, Netherlands, pp. 269–306.

Kiernan, K., Fink, D., Greig, D., Mifud, C., 2010. Cosmogenic radionuclide chronology of pre-last glacial cycle moraines in the Western Arthur Range, Southwest Tasmania. *Quaternary Science Reviews* 29, 3286–3297.

Kukla, G., An, Z. S., Melice, J. L., Gavin, J., Xiao, J. L., 1994. Magnetic susceptibility record of Chinese Loess. *Transactions of the Royal Society of Edinburgh, Earth Science* 81, 263–288.

Lambert, F., Bigler, M., Steffensen, J.P., Hutterli, M., Fischer, H., 2012. Centennial mineral dust variability in high-resolution ice core data from Dome C, Antarctica. *Climate of the Past* 8, 609–623.

Lambert, F., Delmonte, B., Petit, J.R., Bigler, M., Kaufmann, P.R., Hutterli, M.A., Stockler, T.F., Ruth, U., Steffensen, J.P., Maggi, V., 2008. Dust–climate couplings over the past 800,000 years from the EPICA Dome C ice core. *Nature* 452, 616–619.

Lang, N., Wolff, E.W., 2011. Interglacial and glacial variability from the last 800 ka in marine, ice and terrestrial archives. *Climate of the Past* 7, 361–380.

Lewis, A.N., 1945. Pleistocene glaciation in Tasmania. *Papers and Proceedings—The Royal Society of Tasmania* 1944, 41–56.

Lindner, L., Marks, L., 1999. New approach to stratigraphy of palaeolake and glacial sediments of the younger Middle Pleistocene in mid-eastern Poland. *Geological Quarterly* 43(1), 1–8.

Lisiecki, L.E., Raymo, M.E., 2005. A Pliocene–Pleistocene stack of 57 globally distributed benthic δ^{18}O records. *Paleoceanography* 20, PA1003.

Litt, T., Behre, K.-E., Meyer, K.-D., Stephan, H.-J., Wansa, S., 2007. Stratigraphische Begriffe für das Quartär des norddeutschen Vereisungsgebietes. *E&G Quaternary Science Journal* 56, 7–55.

Manabe, S., Broccoli, A.J., 1985. The influence of continental ice sheets on the climate of an ice age. *Journal of Geophysical Research* 90(D1), 2167–2190.

Margari, V., Skinner, L.C., Hodell, D.A., Martrat, B., Toucanne, S., Grimalt, J.O., Gibbard, P.L., Lunkka, J.P., Tzedakis, P.C., 2014. Land-ocean changes on orbital and millennial time scales and the penultimate glaciation. *Geology* 42, 183–186.

Margari, V., Skinner, L.C., Tzedakis, P.C., Ganopolski, A., Vautravers, M., Shackleton, N.J., 2010. The nature of millennial scale climate variability during the past two glacial periods. *Nature Geoscience* 3, 127–131.

Marks, L., 2011. Quaternary glaciations in Poland. In: Ehlers, J., Gibbard, P.L., Hughes, P.D. (Eds.), *Quaternary Glaciations—Extent and Chronology: A Closer Look*. Developments in Quaternary Sciences 15. Elsevier, Amsterdam, pp. 299–304.

McManus, J.F., Oppo, D.W., Cullen, J.L., 1999. A 0.5 million-year record of millennial-scale climate variability in the North Atlantic. *Science* 283, 971–975.

Mercer, J.H., 1984. Simultaneous climatic change in both hemispheres and similar bipolar interglacial warming: evidence and implications. In: Hansen, J.E., Takahashi, T. (Eds.), *Climate Processes and Climate Sensitivity*. Geophysical Monograph Series 29. American Geophysical Union, Washington DC, pp. 307–313.

Mudelsee, M., Schulz, M., 1997. The Mid-Pleistocene transition: onset of 100 ka cycle lags ice volume build-up by 280 ka. *Earth and Planetary Science Letters* 151, 117–123.

Muttoni, G., Carcano, C., Garzanti, E., Ghielmi, M., Piccin, A., Pini, R., Rogledi, S., *et al*. 2003. Onset of Pleistocene glaciations in the Alps. *Geology* 31, 989–992.

Ottesen, D., Dowdeswell, J.A., Bugge, T., 2014. Morphology, sedimentary infill and depositional environments of the Early Quaternary North Sea Basin (56–62 Grad N). *Marine and Petroleum Geology* 56, 123–146.

Pedro, J.B., Jochum, M., Buizert, C., He, F., Barker, S., Rasmussen, S.O., 2018. Beyond the bipolar seesaw: towards a process understanding of interhemispheric cooling. *Quaternary Science Reviews* 192, 27–46.

Peters, J.L., Benetti, S., Dunlop, P., Ó Cofaigh, C., Moreton, S.G., Wheeler, A.J., Clark, C.D., 2016. Sedimentology and chronology of the advance and retreat of the last British–Irish Ice Sheet on the continental shelf west of Ireland. *Quaternary Science Reviews* 140, 101–124.

Pollard, D., DeConto, R.M., 2009. Modelling West Antarctic ice sheet growth and collapse through the past five million years. *Nature* 458, 329–333.

Preusser, F., Graf, H.R., Keller, O., Krayss, E., Schlüchter, C., 2011. Quaternary glaciation history of northern Switzerland. *E&G Quaternary Science Journal* 60, 282–305.

Railsback, L.B., Gibbard, P.L., Head, M.J., Voarintsoa, N.R.G., Toucanne, S., 2015. An optimized scheme of lettered marine isotope substages for the last 1.0 million years, and the climatostratigraphic nature of isotope stages and substages. *Quaternary Science Reviews* 111, 94–106.

https://doi.org/10.1017/qua.2019.76 Published online by Cambridge University Press

Rattenbury, M.S., Townsend, D.B., Johnston, M.R. (compilers), 2006. *Geology of the Kaikoura Area*. Institute of Geological and Nuclear Sciences 1:250,000 Geological Map 13. GNS Science, Lower Hutt, New Zealand.

Raymo, M.E. 1997. The timing of major climate terminations. *Paleoceanography* 12, 577–585.

Rial, J.A., 1999. Pacemaking the ice ages by frequency modulation of Earth's orbital eccentricity. *Science* 285, 564–568.

Richmond, G.M., 1986. Stratigraphy and correlation of glacial deposits of the Rocky Mountains, the Colorado Plateau and the ranges of the Great Basin. *Quaternary Science Reviews* 5, 99–127.

Richmond, G.M., Fullerton, D.S., 1986. Summation of Quaternary glaciations in the United States of America. *Quaternary Science Reviews* 5, 183–196.

Ridgwell, A., Watson, A.J., Raymo, M.E. 1999. Is the spectral signature of the 100 kyr glacial cycle consistent with a Milankovitch origin? *Paleoceanography* 14, 437–440.

Rohling, E.J., Grant, K., Bolshaw, M., Roberts, A.P., Siddall, M., Hemleben, C., Kucera, M., 2009. Antarctic temperature and global sea level closely coupled over the past five glacial cycles. *Nature Geoscience* 2, 500–504.

Rohling, E.J., Grant, K.M., Bolshaw, M., Roberts, A.P., Siddall, M., Hemleben, C., Kucera, M., *et al*., 2014. Sea-level and deep-sea-temperature variability over the past 5.3 million years. *Nature* 508, 477–482.

Roskosch, J., Winsemann, J., Polom, U., Brandes, C., Tsukamoto, S., Weitkamp, A., Bartholomäus, W.A., Henningsen, D., Frechen, M., 2015. Luminescence dating of ice-marginal deposits in northern Germany: evidence for repeated glaciations during the Middle Pleistocene (MIS 12 to MIS 6). *Boreas* 44, 103–126.

Rother, H., Shulmeister, J., Rieser, U., 2010. Stratigraphy, optical dating chronology (IRSL) and depositional model of pre-LGM glacial deposits in the Hope Valley, New Zealand. *Quaternary Science Reviews* 29, 576–592.

Roucoux, K.H., Tzedakis, P.C., de Abreu, L., Shackleton, N.J., 2006. Climate and vegetation changes 180,000 to 345,000 years ago recorded in a deep-sea core off Portugal. *Earth and Planetary Science Letters* 249, 307–325.

Roucoux, K.H., Tzedakis, P.C., Frogley, M.R., Lawson, I.T., Preece, R.C., 2008. Vegetation history of the Marine Isotope Stage 7 interglacial complex at Ioannina, NW Greece. *Quaternary Science Reviews* 27, 1378–1395.

Rovey, C.W., Balco, G., 2011. Summary of Early and Middle Pleistocene glaciations in northern Missouri, USA. In: Ehlers, J., Gibbard, P.L., Hughes, P.D. (Eds.), *Quaternary Glaciations—Extent and Chronology: A Closer Look*. Developments in Quaternary Sciences 15. Elsevier, Amsterdam, pp. 553–561.

Ruddiman, W.F., McIntyre, A., 1982. Severity and speed of Northern Hemisphere glaciation pulses: the limiting case? *Geological Society of America Bulletin* 93, 1273–1279.

Ruddiman, W.F., Raymo, M.E., Martinson, D.G., Clement, B.M., Backman, J., 1989. Pleistocene evolution of Northern Hemisphere climate. *Paleoceanography* 4, 353–412.

Rudenko, T.A., Fainer, Yu.B., Fainer, T.G., 1984. *National Geological Map of the USSR*. 1:1 000 000. New Series, Quadrangle P48,49 (Vanavara). Map of Quaternary Deposits. VSEGEI, Leningrad.

Ruth, U., Bigler, M., Rothlisberger, R., Siggaard-Andersen, M.L., Kipfstuhl, S., Goto- Azuma, K., Hansson, M.E., Johnsen, S.J., Lu, H.Y., Steffensen, J.P., 2007. Ice core evidence for a very tight link between North Atlantic and east Asian glacial climate. *Geophysical Research Letters* 34, L03706.

Schlüchter, C. 1989. A non-classical summary of the Quaternary stratigraphy in the northern Alpine Foreland of Switzerland. *Bulletin de la Société neuchâteloise de géographie* 32–33, 143–157.

Scourse, J.D., Austin, W.E.N., Sejrup, H.P., Ansari, M.H., 1999. Foraminiferal isoleucine epimerization determinations from the Nar Valley Clay, Norfolk, UK: implications for Quaternary correlations in the southern North Sea basin. *Geological Magazine* 136, 543–560.

Sejrup, H.P., Hjelstuen, B.O., Dahlgren, K.I.T., Haflidason, H., Kuijpers, A., Nygård, A., Praeg, D., Stoker, M., Vorren, T.O., 2005. Pleistocene glacial history of the NW European continental margin. *Marine and Petroleum Geology* 22, 1111–1129.

Sejrup, H.P., Larsen, E., Landvik, J., King, E.L., Haflidason, H., Nesje, A., 2000. Quaternary glaciations in southern Fennoscandia: evidence from southwestern Norway and the northern North Sea region. *Quaternary Science Reviews* 19, 667–685.

Shackleton, N.J., 1967. Oxygen isotope analyses and Pleistocene temperatures re-assessed. *Nature* 215, 15–17.

Shakun, J.D., Lea, D.W., Lisiecki, L.E., Raymo, M.E., 2015. An 800-kyr record of global surface ocean $\delta^{18}O$ and implications for ice volume-temperature coupling. *Earth and Planetary Science Letters* 426, 58–68.

Singer, B., Ackert, R.P., Guillou, H., 2004. $^{40}Ar/^{39}Ar$ and K-Ar chronology of Pleistocene glaciations in Patagonia. *Geological Society of America Bulletin* 116, 434–450.

Singer, B.S., Jicha, B.R., Mochizuki, N., Coe, R.S., 2019. Synchronizing volcanic, sedimentary, and ice core records of Earth's last magnetic polarity reversal. *Science Advances* 5, 8, eaaw4621.

Sosdian, S., Rosenthal, Y., 2009. Deep-sea temperature and ice volume changes across the Pliocene-Pleistocene climate transitions. *Science* 325, 306–310.

Spooner, I.S., Osborn, D.G., Barendregt, R.W., Irving, E., 1996. A Middle Pleistocene (isotope stage 10) glacial sequence in the Stikine River valley, British Columbia. *Canadian Journal of Earth Sciences* 33, 1428–1438.

Spratt, R.M., Lisiecki, L.E., 2016. A Late Pleistocene sealevel stack. *Climate of the Past* 12, 1079–1092.

Stephan, H.-J., 2014. Climato-stratigraphic subdivision of the Pleistocene in Schleswig-Holstein, Germany and adjoining areas. *E&G Quaternary Science Journal* 63, 3–18.

Stiff, B.J., Hansel, A.K., 2004. Quaternary glaciations in Illinois. In: Ehlers, J., Gibbard, P.L. (Eds.), *Quaternary Glaciations—Extent and Chronology*. Part 2, *North America*. Developments in Quaternary Sciences 2. Elsevier, Amsterdam, pp. 71–82.

Stocker, T.F., Johnsen, S.J., 2003. A minimum thermodynamic model for the bipolar seesaw. *Paleoceanography* 18, 1087.

Stoker, M.S., Bradwell, T., 2005. The Minch palaeo-ice stream, NW sector of the British-Irish ice sheet. *Journal of the Geological Society of London* 162, 425–428.

Stokes, C., Tarasov, L., Dyke, A.S., 2012. Dynamics of the North American Ice Sheet complex during its inception and build-up to the Last Glacial Maximum. *Quaternary Science Reviews* 50, 86–104.

Sugden, D.E., Bentley, M.J., Ó Cofaigh, C., 2006. Geological and geomorphological insights into Antarctic ice sheet evolution. *Philosophical Transactions of the Royal Society of London A* 364, 1607–1625.

Sutter, J., Fischer, H., Grosfeld, K., Karlsson, N.B., Kleiner, T., Van Liefferinge, B., Eisen, O., 2019. Modelling the Antarctic Ice Sheet across the mid-Pleistocene transition—implications for oldest ice. *Cryosphere* 13, 2023–2041.

https://doi.org/10.1017/qua.2019.76 Published online by Cambridge University Press

Svendsen, J.I., Alexanderson, H., Astakhov, V.I., Demidov, I., Dowdeswell, J.A., Funder, S., Gataullin, V., *et al*., 2004. Late Quaternary ice sheet history of northern Eurasia. *Quaternary Science Reviews* 23, 1229–1271.

Swanger, K.M., Lamp, J.L., Winckler, G., Schaefer, J.M., Marchant, D.R., 2017. Glacier advance during Marine Isotope Stage 11 in the McMurdo Dry Valleys of Antarctica. *Scientific Reports* 7, 41433.

Swingedouw, D., Fichefet, T., Goosse, H., Loutre, M.F., 2009. Impact of transient freshwater releases in the Southern Ocean in the AMOC and climate. *Climate Dynamics* 33, 365–381.

Syverson, K.M., Colgan, P.M., 2004. The Quaternary of Wisconsin: a review of stratigraphy and glaciation history. In: Ehlers, J., Gibbard, P.L. (Eds.), *Quaternary Glaciations—Extent and Chronology*. Part 2, *North America*. Elsevier, Amsterdam, pp. 295–311.

Syverson, K.M., Colgan, P.M., 2011. The Quaternary of Wisconsin: an updated review of stratigraphy, glacial history and landforms. In: Ehlers, J., Gibbard, P.L., Hughes, P.D. (Eds.), *Quaternary Glaciations—Extent and Chronology: A Closer Look*. Developments in Quaternary Sciences 15. Elsevier, Amsterdam, pp. 537–552.

Tabor, C.R., Poulsen, C.J., 2016. Simulating the mid-Pleistocene transition through regolith removal. *Earth and Planetary Science Letters* 434, 231–240.

Thierens, M., Pirlet, H., Colin, C., Latruwe, K., Vanhaecke, F., Lee, J.R., Stuut, J.-B., *et al*., 2012. Ice-rafting from the British-Irish ice sheet since the earliest Pleistocene (2.6 million years ago): implications for long-term mid-latitudinal ice-sheet growth in the North Atlantic region. *Quaternary Science Reviews* 44, 229–240.

Toucanne, S., Zaragosi, S., Bourillet, J.F., Cremer, M., Eynaud, F., Van Vliet-Lanoe, B., Penaud, A., *et al*., 2009a.Timing of massive "Fleuve Manche" discharges over the last 350 kyr: insights into the European ice-sheet oscillations and the European drainage network from MIS 10 to 2. *Quaternary Science Reviews* 28, 1238–1256.

Toucanne, S., Zaragosi, S., Gibbard, P.L., Bourillet, J.F., Cremer, M., Eynaud, F., Giraudeau, J., *et al*., 2009b. A 1.2 my record of glaciation and fluvial discharge from the West European continental margin. *Quaternary Science Reviews* 28, 2974–2981.

Van Husen, D., Reitner, J.M., 2011. An outline of the Quaternary stratigraphy of Austria. *E&G Quaternary Science Journal* 60, 366–387.

Velichko, A.A., Faustova, M.A., Pisareva, V.V., Gribchenko, Y.N., Sudakova, N.G., Lavrentiev, N.V., 2011. Glaciations of the East European Plain—distribution and chronology. In: Ehlers, J., Gibbard, P.L., Hughes, P.D. (Eds.), *Quaternary Glaciations—Extent and Chronology—A Closer Look*. Developments in Quaternary Sciences 15. Elsevier, Amsterdam, pp. 337–360.

Vidal Romaní, F., Mosquera, D., Marti, K., 2015. The glaciation of Serra de Quiexa-Invernadoiro and Serra do Gerês, NW Iberia. A critical review and a cosmogenic nuclide (^{10}Be and ^{21}Ne) chronology. *Cadernos Laboratorio Xeolóxico de Laxe* 38, 27–45.

Waelbroeck, C., Labeyrie, L., Michel, E., Duplessy, J.C., McManus, J.F., Lambeck, K., Balbon, E., Labracherie, M., 2002. Sea-level and deep water temperature changes derived from benthic foraminifera isotopic records. *Quaternary Science Reviews* 21, 295–305.

Ward, B.C., Bond, J.D., Froese, D., Jensen, B., 2008. Old Crow tephra (14010 ka) constrains penultimate Reid glaciation in central Yukon Territory. *Quaternary Science Reviews* 27, 1909–1915.

White, T.S., Bridgland, D.R., Howard, A.J., Westaway, R., White, M.J., 2010. Evidence from the Trent terrace archive, Lincolnshire, UK, for lowland glaciation of Britain during the Middle and Late Pleistocene. *Proceedings of the Geologists' Association* 121, 141–153.

White, T.S., Bridgland, D.R., Westaway, R., Straw, A., 2017. Evidence for a late Middle Pleistocene glaciation of the British margin of the southern North Sea. *Journal of Quaternary Science* 32, 261–275.

Willeit, M., Ganopolski, A., Calov, R., Brovkin, V., 2019. Mid-Pleistocene transition in glacial cycles explained by declining CO_2 and regolith removal. *Science Advances* 5, eaav7337.

https://doi.org/10.1017/qua.2019.76 Published online by Cambridge University Press